JOURNAL OF GEOPHYSICAL RESEARCH, VOL. 113, B09308, doi:10.1029/2007JB005239, 2008

Inversion of seismic and geodetic data for the major element chemistry and temperature of the Earth's mantle

A. Khan,[1,2] J. A. D. Connolly,[3] and S. R. Taylor[4]

Received 20 June 2007; revised 17 April 2008; accepted 30 May 2008; published 16 September 2008.

[1] We jointly invert global seismic traveltime data, mean mass, and mean moment of inertia for Earth's mantle composition and thermal state using a stochastic sampling algorithm. The chemical composition of the silicate Earth is modeled within the system CaO-FeO-MgO-Al_2O_3-SiO_2. Given these parameters we calculate the stable mineralogy and its elastic properties and density as a function of pressure and temperature using Gibbs free energy minimization. Bulk seismic *P* and *S* wave velocity profiles (V_P, V_S) are computed from Voigt-Reuss-Hill averaging, while anelastic contributions to V_P and V_S are calculated assuming shear attenuation to be linearly varying with depth. From these radial profiles, seismic traveltimes, mean mass, and mean moment of inertia are calculated, providing a range of compositions and temperatures that fit data within uncertainties. Specifically, we find an upper mantle composition that is depleted in CaO and Al_2O_3 relative to canonical values inferred for the upper mantle from analysis of mantle xenoliths. The lower mantle in contrast is found to be enriched in FeO and depleted in SiO_2, with a Mg/Si ratio of ~1.2 and a Mg# of ~0.83, resulting in a bulk silicate Earth composition that is unmatched by any of the common chondrites. The mantle geotherm is found to be superadiabatic for depths >1200 km, while lower mantle temperatures reach ~2400°C at 2500 km depth. The presence of a chemical transition between upper and lower mantle is further suggested in the depth range 650–750 km.

Citation: Khan, A., J. A. D. Connolly, and S. R. Taylor (2008), Inversion of seismic and geodetic data for the major element chemistry and temperature of the Earth's mantle, *J. Geophys. Res.*, *113*, B09308, doi:10.1029/2007JB005239.

1. Introduction

[2] Knowledge of the internal constitution of the planets is crucial to our understanding of the origin and evolution of our solar system. By far the largest insights into the physical structure of the Earth have come from geophysical analyzes, and seismology in particular. However, as seismology is only an indirect means of obtaining information on the fundamental parameters (composition and geotherm), combining seismic velocity models with results and data from geodynamic modeling, mineral physics, mantle petrology and geochemical analyzes of primitive meteorites, mantle xenoliths and mantle-derived magmas, has gained considerably in importance since the work of *Birch* [1952], and includes a wide variety of studies [e.g., *Anderson*, 1989; *Ita and Stixrude*, 1992; *Sobolev and Babeyko*, 1994; *Fabrichnaya and Kuskov*, 1994; *Goes et al.*, 2000; *Connolly and Kerrick*, 2002; *Cammarano et al.*, 2005; *Mattern et al.*, 2005; *Ricard et al.*, 2005; *Stixrude and Lithgow-Bertelloni*, 2005a, 2005b; *Kuskov et al.*, 2006; *Khan et al.*, 2006a, 2006b, 2006c; *Matas et al.*, 2007].

[3] For some decades now a number of seismic profiles, such as the 1D radial profiles, Preliminary Reference Earth Model (PREM) [*Dziewonski and Anderson*, 1981] and AK135 [*Kennett et al.*, 1995], have formed the basis for interpreting the constitution of the Earth. The pyrolite model of Ringwood [e.g., *Ringwood*, 1975], for example, has become widely acknowledged as being representative of the Earth's average upper mantle composition, because of its ability to satisfy a large range of geochemical and geophysical data, such as the aforementioned 1D seismic reference models, within uncertainties of the seismic models and the minerals physics data. In addition, recent electromagnetic sounding studies are also found to be consistent with the pyrolite model [e.g., *Xu et al.*, 2003; *Dobson and Brodholt*, 2000], although more chondritic lower mantle compositions are not ruled out [*Khan et al.*, 2006b]. In spite of the pyrolite models overall good fit to data, a number of issues are as yet unresolved. For example, can this model composition along an adiabatic temperature gradient explain the observed variations in sufficient detail, and if present, how significant are any deviations? Moreover, can we explain the observed seismic discontinuities, notably the 660, as being due to a change of phase in an isochemical mantle or is a chemical change called for; and how does this relate to the observation that some slabs are seen to stop at ~1200 km depth above the core mantle boundary [*van der*

---

[1] Niels Bohr Institute, University of Copenhagen, Copenhagen, Denmark.

[2] On leave at Institute of Geophysics, Swiss Federal Institute of Technology, Zurich, Switzerland.

[3] Earth Sciences Department, Swiss Federal Institute of Technology, Zurich, Switzerland.

[4] Department of Earth and Marine Sciences, The Australian National University, Canberra, Australia.

0148-0227/08/2007JB005239$09.00

Hilst et al., 1997], which has fueled speculation of chemical layering deep within the mantle [*Kellogg et al.*, 1999; *Anderson*, 2002].

[4] Intimately related to the outstanding and still much debated question of mantle chemical stratification [e.g., *Helffrich and Wood*, 2001] is the question of the possible building blocks of the terrestrial planets, and in particular of the Earth [e.g., *Drake and Righter*, 2002]. The composition of peridotites, which are samples from the upper mantle and have been used to infer its composition [*Jagoutz et al.*, 1979; *McDonough and Sun*, 1995; *Lyubetskaya and Korenaga*, 2007], are found to be depleted in Si relative to the chondrites. The latter are traditionally thought of as the building blocks of the terrestrial planets, as the chondrites appear to sample the primitive material that started out as dust in the solar nebula and which grew, through collisional processes [e.g., *Weidenschilling*, 2000], into planets. A possible solution to the conundrum of Si depletion, then, is to propose that it has been sequestered into the core and/or lower mantle [e.g., *Poirier*, 1994; *Allegre et al.*, 1995]. The resolution of the lower mantle Si content, or the bulk mantle composition in general, thus holds the potential of providing insight into the nature of the material from which the Earth assembled.

[5] Relying on laboratory mineral physics data, a number of recent studies have attempted to bridge the inherent shortcoming in first obtaining profiles from seismic tomography studies and then interpreting these in terms of compositional and thermal variations by trying to directly link mineral physics data with geophysical observations to provide compositional and thermal constraints on the Earth's mantle [e.g., *Matas et al.*, 2007; *Cammarano et al.*, 2005; *Deschamps and Trampert*, 2004; *Mattern et al.*, 2005; *Stixrude and Lithgow-Bertelloni*, 2005a, 2005b; *Trampert et al.*, 2004; *Marton and Cohen*, 2002; *da Silva et al.*, 2000; *Jackson*, 1998]. These studies in some form or another only address aspects of the fundamental problem of constraining composition and thermal state from a set of geophysical data. Cammarano et al., for example, use a model of physical properties which is supplemented with an account of phase equilibria from a graphical summary of experimental data, thereby being confined to a single composition. The approach of *Matas et al.* [2007], while being thermodynamically self-consistent á la *Stixrude and Lithgow-Bertelloni* [2005a, 2005b] or *Connolly and Kerrick* [2002], is restricted to inversion of preexisting seismic velocity profiles (AK135), rather than the data from which the former are derived, thereby adopting its parameterization and unspecified uncertainties. In addition, the highly nonlinear inverse problem posed, is typically solved using either deterministic methods or purely random search techniques. As an example, *Matas et al.* use the least squares criterion of *Tarantola and Valette* [1982a], which, however, is not designed to handle the strong nonlinearities in the present class of problems [e.g., *Tarantola*, 2004]. *Deschamps and Trampert* [2004] and *Cammarano et al.* [2005], meanwhile, try to exhaustively search a high-dimensional model space. Apart from the fact that this is presently not possible, there is no resampling of the outcome to ensure that it is distributed according to the posterior. The approach taken by *Stixrude and Lithgow-Bertelloni* [2005a, 2007], on the other hand, is elegant, but is limited to a single forward model, and does not address fundamental geophysical observations.

[6] With this in mind and given the caveats of previous studies, it is the purpose here to jointly invert seismic data (global ISC *P* and *S* wave traveltimes [*Engdahl et al.*, 1998]) and geodetic data (mean mass and moment of inertia [*Chambat and Valette*, 2001]) for Earth's mantle composition and thermal state. Our approach is based on the thermodynamic self-consistent phase equilibrium calculation of *Connolly* [2005], which provides a unified description of elasticity and phase equilibria of multicomponent and multiphase assemblages, and allows us to construct models of the interior of planets where mineralogy and elastic wave velocity variations are specified as functions of pressure and temperature. This method is combined with a fully nonlinear stochastic sampling algorithm, based on a Markov chain Monte Carlo (MCMC) method, to rigorously invert geophysical data for Earth's mantle geotherm and composition within the system CaO-FeO-MgO-Al_2O_3-SiO_2. The importance of this approach has been exemplified in our previous work with applications to the Earth, Moon and Mars (*Khan et al.* [2006a, 2006b, 2006c], *Khan and Connolly* [2008], as well as in the studies by *Stixrude and Lithgow-Bertelloni* [2005a, 2007]). We will further illustrate the significance of considering phase equilibria in geophysical applications by specifically analyzing two models that although very similar in composition and mantle temperature, nonetheless differ in calculated phase equilibria. In particular, we will show that while differences in physical properties of the two assemblages estimated from the phase equilibria are subtle, they nonetheless produce geophysical responses that are distinguishable within the uncertainties of geophysical data.

[7] As mentioned, the inverse problem posed here is strongly nonlinear and to treat it in a fully nonlinear way, we employ the Bayesian approach as formulated by *Tarantola and Valette* [1982b] and *Mosegaard and Tarantola* [1995]. For this class of inverse (henceforth general inverse) problems the shape of the posterior probability density (the solution models) in the model space is complex and is in general inadequately described using typically employed measures such as means and covariances. Instead we present the solution in terms of a large collection of models sampled from the posterior probability density using a Monte Carlo algorithm. While this algorithm is based on a random sampling of the model space, only models that result in a good data fit and are consistent with prior information are frequently sampled. Applications of stochastic sampling algorithms in geophysics and elsewhere are numerous. For reviews the interested reader is referred to, e.g., *Mosegaard* [1998] and *Mosegaard and Sambridge* [2002], while a very thorough and eloquently worked geophysical example can be found in *Bosch* [1999].

2. Mantle Composition and Geotherm: A Summary of Previous Studies

[8] As noted in the introduction a number of studies have attempted to constrain mantle composition and geotherm using both forward and inverse approaches, in combination with thermodynamic data, i.e., elastic parameters, acquired from laboratory measurements as well as ab initio calcu-

Table 1. Summary of Previous Studies Trying to Constrain Compositional and Thermal Parameters[a]

Author	T_{660} (K)	T_{CMB} (K)	∇T_{LM}	Lower Mantle Mineralogy	Observational Constraints	Method	Mineralogical Model/Compositional Dependence	Chemical System
Matas et al.	1935[b]	2972	superad.	cosmic	v_P, v_S and ρ from AK135	inversion using least squares criterion	thermodynamic/yes	CFMAS
	1926[b]	2942	superad.	chondritic				
	1875[b]	2702	superad.	pyrolitic				
Khan et al.	1900	3200	superad.	chondritic	Electromagnetic sounding data, mass and moment of inertia	MCMC inversion	thermodynamic/yes	CFMAS
Mattern et al.	1800	2000	subad.	pyrolite	v_ϕ and ρ from PREM and AK135	as Matas et al.	thermodynamic/yes	CFMAS
	2200	2500	subad.	perovskite-rich				
	2500	2700	subad.	cosmic				
Cammarano et al.	1873	2400	ad.	pyrolite	Global *P* and *S* traveltimes, fundamental normal modes and mass	random sampling	parameterized phase diagram/no	CFMAS
Deschamps and Trampert	3300	4200	superad.	pyrolitic	v_P and v_S from PREM	random sampling	parameterized phase diagram/yes	FMS
Marton and Cohen	1800	2400	ad.	pyrolitic	v_P, v_S and ρ from PREM and AK135f	forward model (ab initio)	parameterized phase diagram/no	CFMAS
da Silva et al.	1900	4000	superad.	pyrolite	K_S from PREM	forward model (ab initio)	parameterized phase diagram/no	CFMAS
Jackson et al.	1850	2300	ad	pyrolitic	as Mattern et al.	forward model	parameterized phase diagram/no	FMS

[a] Only summary values are presented, i.e., uncertainties are not indicated. For this and other modeling/technical details the reader is referred to the individual studies.

lations. Rather than provide a detailed review of these investigations, we have summarized their results in table format (see Table 1). However, a word of caution needs to be appended. Different authors have used (1) different databases, i.e., elastic parameters, (2) different observational constraints, (3) different equations of state, as well as other modeling assumptions, and (4) different inversion schemes (where applied) and unless these premises are carefully analyzed, direct comparison is difficult. In spite of these reservations, it appears that little consensus exists with regard to mantle composition and thermal state. While pyrolite seems to be a preferred composition, it is by no means unique. For example, *Cammarano et al.* [2005], constrained their lower mantle composition to pyrolite. Combining this composition with the adiabatic mantle geotherm of *Brown and Shankland* [1981], however, severely restricted their ability to fit the global traveltime data and led them to suggest that other possible compositions cannot be ruled out. *Matas et al.* [2007] meanwhile, using more leniency as regards composition and geotherm, but using preexisting velocity profiles as ground truth, obtained Mg/Si ratios, depending on modeling assumptions, between 1.03 and 1.18 with uncertainties in the range of 0.15. Equally little consensus surrounds the lower mantle thermal gradient, i.e., whether it is subadiabatic, superadiabatic, or simply adiabatic, although judging by the most recent investigations a superadiabatic lower mantle thermal gradient seems favored [*Matas et al.*, 2007; *Khan et al.*, 2006b; *Cammarano et al.*, 2005; *Deschamps and Trampert*, 2004].

3. The Inverse Problem

3.1. Statement and Solution of the General Inverse Problem

[9] For a general inverse problem the relationship between model **m** and data **d** is usually written as

$$\mathbf{d} = \mathrm{g}(\mathbf{m}) \tag{1}$$

where g is a typically nonlinear operator. Central to the formulation of the Bayesian approach to inverse problems as delineated by *Tarantola and Valette* [1982b] is the extensive use of probability density functions (pdf's) to describe any piece of information that enters the problem. These pdf's include

[10] 1. probabilistic prior information on model and data parameters, $\eta(\mathbf{m})$ (for the present brief discussion we limit ourselves to a functional dependence on **m** and omit any reference to **d**).

[11] 2. the physical laws that relate data to the model parameters which are sought.

[12] These pdf's are then combined using Bayes theorem to yield the posterior pdf in the model space

$$\sigma(\mathbf{m}) = k\eta(\mathbf{m})\mathcal{L}(\mathbf{m}), \tag{2}$$

where k is a normalization constant and $\mathcal{L}(\mathbf{m})$ is the likelihood function and can, in probabilistic terms, be interpreted as a measure of data misfit between observed data and data calculated from model **m**.

[13] In the present formulation we are considering different sets of model parameters, describing a combined compositional/thermal-physical model of the Earth. The compositional/thermal parameters are the fundamental ones. We label these primary parameters ($\mathbf{m}_p$). The parameters describing the physical properties could be seismic wave velocities and electrical conductivities, and are termed secondary parameters ($\mathbf{m}_s$). In the joint model space we thus have $\mathbf{m} = \{\mathbf{m}_p, \mathbf{m}_s\}$. Extending equation (2) to the present joint model parameter description (for details, see *Khan et al.* [2006a]), we obtain the following composite posterior pdf

$$\sigma(\mathbf{m}_s, \mathbf{m}_p) = k\eta(\mathbf{m}_s, \mathbf{m}_p)\mathcal{L}(\mathbf{m}_s, \mathbf{m}_p) \tag{3}$$

which can be decomposed into

$$\sigma(\mathbf{m}_s, \mathbf{m}_p) = k\eta_s(\mathbf{m}_s|\mathbf{m}_p)\eta_p(\mathbf{m}_p)\mathcal{L}_s(\mathbf{m}_s|\mathbf{m}_p)\mathcal{L}_p(\mathbf{m}_p) \tag{4}$$

where k is a normalization constant, $\eta_p(\mathbf{m}_p)$ the prior pdf containing information on primary model parameters only, $\eta_s(\mathbf{m}_s|\mathbf{m}_p)$ a conditional prior pdf and describes prior knowledge on $\mathbf{m}_s$ as well as the dependence of $\mathbf{m}_s$ on $\mathbf{m}_p$, $\mathcal{L}_p(\mathbf{m}_p)$ the likelihood function that calculates secondary model parameters given values of primary model parameters and $\mathcal{L}_s(\mathbf{m}_s|\mathbf{m}_p)$ another likelihood function that calculates data given values of $\mathbf{m}_s$, conditional on $\mathbf{m}_p$. Sections 4.1 to 4.3 detail $\mathcal{L}_p$ and $\mathcal{L}_s$, whereas η_p and η_s are considered in sections 5.1.1 to 5.1.5.

3.2. Monte Carlo Sampling of the Posterior Distribution

[14] Having defined the posterior distribution above (equation (4)) as the solution to our inverse problem, let us turn to the problem of actually obtaining $\sigma(\mathbf{m})$. In the case of the general inverse problem, however, the posterior pdf does not exist as an analytical function and given its usually complex shape defined over a high-dimensional model space it cannot be integrated analytically. Instead we have to estimate posterior probabilities by statistical integration methods and the basic idea is to design a random walk in the model space, that, if unmodified, samples some initial probability distribution. By subsequently applying certain probabilistic rules, we can modify the random walk in such a way that it will sample some target distribution. The Metropolis-Hastings algorithm [*Metropolis et al.*, 1953; *Hastings*, 1970], is a MCMC method, which can be shown to be the one that most efficiently achieves this goal. The MCMC method is so named, because it employs a random number generator (Monte Carlo) and has got shortest possible memory, that is, each step is only dependent upon the previous step (Markov chain). This is contained in the following algorithm [e.g., *Mosegaard*, 1998]

[15] **Algorithm**. If we have a random function $\mathcal{K}(\mathbf{m}^n)$ which samples the prior probability density $\eta(\mathbf{m})$ iteratively ($\mathbf{m}^{n+1} = \mathcal{K}(\mathbf{m}^n)$), and a random function $\mathcal{F}$ generating a uniformly distributed random number from the interval [0, 1], the random function Ξ, which iteratively operates on the current parameter vector $\mathbf{m}^n$ and produces the next parameter vector $\mathbf{m}^{n+1}$

$$\mathbf{m}^{n+1} = \Xi(\mathbf{m}^n) = \begin{cases} \mathcal{K}(\mathbf{m}^n) & \text{if } \mathcal{F} \leq \min\left[1, \frac{\mathcal{L}(\mathcal{K}(\mathbf{m}^n))}{\mathcal{L}(\mathbf{m}^n)}\right], \\ \mathbf{m}^n & \text{else.} \end{cases}$$

samples the probability density $\sigma(\mathbf{m}) = k\eta(\mathbf{m})\mathcal{L}(\mathbf{m})$.

[16] In addition, $\mathcal{K}$ has to satisfy the following two constraints, 1. given enough iterations, access to all points $\mathbf{m}$ in the parameter space must be ensured through the iterative procedure and 2. successive visits (or more) to the same point are possible, i.e., $\mathbf{m}^n = \mathcal{K}(\mathbf{m}^n)$.

[17] Of importance here, is that this algorithm renders us capable of sampling the space with a sampling density proportional to the given probability density without excessively sampling low-probability areas of the model space. This is especially important when we are concerned with high-dimensional spaces, where a large proportion of the volume may have near-zero probability density. It might be noted that exhaustive sampling, where all points in a dense grid covering the model space, are visited in a random fashion, is the simplest method, but is useless for problems with more than 10 parameters [*Tarantola*, 2004], and thus most geophysical applications.

[18] The solution to the general inverse problem, as presented here, cannot be described by one single realization like the mean, the median model or the maximum likelihood model, but is best characterized by looking at samples from the posterior pdf. One possibility is to calculate resolution measures, which are easily evaluated from [e.g., *Mosegaard*, 1998]

$$\mathcal{R}(\Lambda,f) = \int_\Lambda f(\mathbf{m})\sigma(\mathbf{m})d\mathbf{m} \approx \frac{1}{N}\sum_{\{n|\mathbf{m}_n\in\Lambda\}} f(\mathbf{m}_n) \qquad (5)$$

where $f(\mathbf{m})$ is a given function of the model parameters $\mathbf{m}$, Λ is an event or subset of the model space containing the models of current interest and N is the total number of samples taken from Λ.

4. Constructing the Forward Model

[19] Equation (1) describes in short-hand notation how we calculate data from model parameters. Let us take a somewhat more detailed look at this by splitting equation (1) into the following set of model parameter vectors $\mathbf{m}_i$, data vectors $\mathbf{d}_j$ and forward operators g_i

$$\begin{tikzcd} & & \mathbf{m}_4 \arrow[r, "g_3"] & \mathbf{m}_5 \arrow[r, "g_4"] & \mathbf{m}_6 \arrow[r, "g_5"] & \mathbf{d}_2 \\ \mathbf{m}_1 \arrow[r, "g_1"] & \mathbf{m}_2 \arrow[ur, "g_2"] \arrow[r, "g_2"] & \mathbf{m}_3 \arrow[ur, "g_3"] \arrow[r, "g_6"] & \mathbf{d}_1 \end{tikzcd}$$

where specifically the model parameter vectors $\mathbf{m}_i$ correspond to

[20] $i = 1$: starting composition and geotherm,

[21] $i = 2$: modal mineralogy,

[22] $i = 3$: bulk density,

[23] $i = 4$: bulk elastic moduli,

[24] $i = 5$: bulk elastic P and S wave velocities and attenuation model Q,

[25] $i = 6$: bulk anelastic P and S wave velocities.and where the forward operators g_k calculate

[26] $k = 1$: equilibrium modal mineralogy using Gibbs free energy minimization,

[27] $k = 2$: bulk physical properties using Voigt-Reuss-Hill averaging,

[28] $k = 3$: bulk elastic P and S wave velocities,

[29] $k = 4$: bulk anelastic P and S wave velocities,

[30] $k = 5$: P and S wave traveltimes

[31] $k = 6$: mean mass and moment of inertia,and finally, where the data vectors $\mathbf{d}_j$ contain

[32] $j = 1$: mean mass and moment of inertia.

[33] $j = 2$: global P and S wave traveltimes,

[34] Note that $\mathbf{m}_{2,\ldots,6}$ are all functions of radius. The g's will be described briefly in the following.

4.1. Solving the Forward Problem I: Thermodynamical Modeling of Physical Properties

[35] Mantle compositions were explored within the system CaO-FeO-MgO-Al_2O_3-SiO_2, a chemical model that is thought to account for more than 98% of the mass of the mantle [e.g., *Irifune*, 1994] and provide an adequate model

Table 2. Phase Notation, Formulae, and Solution Model Sources[a]

Symbol	Phase	Formula	Source
ca-pv	Calcium-perovskite	CaO	
Cpx	Clinopyroxene	$Ca_{2y}Mg_{4-2x-2y}Fe_{2x}Si_4O_{12}$	[1]
Gt	Garnet	$Fe_{3x}Ca_{3y}Mg_{3(1-x+y+z/3)}Al_{2-2z}Si_{3+z}O_{12}$, $x + y + 4z/3 \leq 1$	[1]
Ol	Olivine	$[Mg_xFe_{1-x}]_2SiO_4$	[1]
Opx	Orthopyroxene	$[Mg_xFe_{1-x}]_{4-2y}Al_{4(1-y)}Si_4O_{12}$	[1]
Sp	Spinel	$Mg_xFe_{1-x}Al_2O_3$	[1]
C2/c	Pyroxene	$[Mg_xFe_{1-x}]_4Si_4O_{12}$	[1]
Aki	Akimotoite	$[Mg_xFe_{1-x}]_{1-y}Al_{2y}Si_{1-y}O_3$	[2]
Pv	Perovskite	$[Mg_xFe_{1-x}]_{1-y}Al_{2y}Si_{1-y}O_3$	[2]
Ppv	Post-perovskite	$[Mg_xFe_{1-x}]_{1-y}Al_{2y}Si_{1-y}O_3$	[3]
Ring	Ringwoodite	$[Mg_xFe_{1-x}]_2SiO_4$	[1]
Wad	Wadsleyite	$[Mg_xFe_{1-x}]_2SiO_4$	[1]
Wus	Wuestite	$Mg_xFe_{1-x}O$	[2]

[a] Unless otherwise noted, the compositional variables x, y, and z may vary between zero and unity and are determined as a function of the computational variables by free-energy minimization. Sources: (1) *Stixrude and Lithgow-Bertelloni* [2005a]; (2) *Fabrichnaya* [1998]; (3) *Ono and Oganov* [2005].

for its seismic structure [e.g., *da Silva et al.*, 2000] and electrical conductivity [e.g., *Xu et al.*, 2003; *Khan et al.*, 2006b]. The mantle mineralogy was assumed to be dictated by thermodynamic equilibrium and was computed from thermodynamic data for a given pressure, temperature and bulk composition by Gibbs energy minimization as described by *Connolly* [2005]. These calculations, taking into consideration the phases summarized in Table 2, yielded the amounts, compositions and thermodynamic properties, including elastic moduli, of the stable phases. To avoid the necessity of assuming a model for mantle rock texture, the aggregate adiabatic bulk and shear moduli used for the estimation of seismic velocities were estimated by Voigt-Reuss-Hill averaging.

[36] The calculations were made using the equation of state (EoS) and parameterization of *Stixrude and Lithgow-Bertelloni* [2005a] augmented by *Khan et al.* [2006b] for the end-member compositions of the lower mantle phases magnesiowüstite, perovskite, postperovskite and Ca-perovskite.

[37] Components not considered include Na_2O, TiO_2, Cr_2O_3 and H_2O, because of a lack thermodynamic data. These less abundant elements are most likely to affect locations of phase boundaries, rather than physical properties, as discussed by *Stixrude and Lithgow-Bertelloni* [2005a].

4.2. Solving the Forward Problem II: Anelasticity and Traveltimes

[38] It has been argued that effects arising from the viscoelastic behavior of materials at elevated temperatures, i.e., attenuation and dispersion, could be potentially important in the interpretation of seismic velocities in tomography images [*Matas and Bukowinski*, 2007; *Brodholt et al.*, 2007]. Traditionally, global models (1D) of attenuation (Q) have been obtained from the analysis of surface wave and normal mode data [e.g., *Anderson and Hart*, 1978; *Dziewonski and Anderson*, 1981; *Widmer et al.*, 1991; *Durek and Ekström*, 1996], as well as differential attenuation measurements of S and ScS phases [*Lawrence and Wysession*, 2006]. For a recent review the reader is referred to *Romanowicz and Durek* [1999]. It has been found experimentally that attenuation Q or its inverse, the quality factor, is strongly temperature dependent, and in the case of shear (bulk attenuation is assumed to be less significant with values ranging from $\sim 10^3 - 10^4$ [*Durek and Ekström*, 1996]) follows an Arrhenius type law of the form [e.g., *Karato*, 1993]

$$Q_\mu = Q_0 \exp\left[\frac{\alpha(E + pV)}{RT}\right] \tag{6}$$

where Q_0 is a constant, E activation energy, V activation volume, p pressure, T temperature, R the gas constant and α an exponent, which, for seismic waves, has been determined experimentally to be between 0.15–0.25 [*Jackson et al.*, 2002] and between 0.1–0.4 theoretically [*Minster and Anderson*, 1981]. The physical processes giving rise to attenuation in rocks (grain boundary processes, dislocation motion), as well as their experimental determination, is reviewed by, e.g., *Karato and Spetzler* [1990]. That Q is weakly frequency dependent throughout most of the mantle, is in line with the absorption band model, where attenuation is modeled as arising from a broad distribution of thermally activated relaxation processes [e.g., *Kanamori and Anderson*, 1977; *Minster and Anderson*, 1981; *Anderson and Given*, 1982].

[39] A consequence of a dissipative system is the presence of velocity dispersion due to attenuation. Given a model of Q_μ ($= Q_S$) and assuming a weakly frequency dependent Q ($Q \propto \omega^\alpha$, $0 < \alpha < 1$, [*Karato and Spetzler*, 1990]), anelastic shear velocities V are determined according to the model of *Minster and Anderson* [1981]

$$V(p,T,X) = v(p,T,X)\left[1 - \frac{2Q^{-1}}{\tan(\alpha\pi/2)}\right] \tag{7}$$

where v is the anharmonic velocity as a function of p, T and composition X obtained in section 4.1. P wave velocities are obtained by replacing Q_S^{-1} by $Q_P^{-1} = (4V_S^2/3V_P^2)Q_\mu^{-1}$, where contributions from bulk attenuation Q_κ have been disregarded (typically $Q_\kappa \rightarrow \infty$ [*Romanowicz and Durek*, 1999]).

[40] To calculate anelastic velocities from equation (7), it would be straightforward to employ equation (6) to estimate radial shear and bulk attenuation models using the radial pressure and temperature profiles from the thermodynamic calculation (section 4.1). However, rather than use equation

(6), because of the present scarcity of measurements of α, E and V for individual minerals (some experimentally determined activation energies for perovskite and periclase can be found in the work of *Brodholt et al.* [2007]), we model Q as a linear function of depth, i.e., $Q(r) = Q_0 + \nabla_r Q \cdot r$, where Q_0 is the value of Q at the surface, $\nabla_r Q$ is the radial gradient in Q and r radius. Q_0, $\nabla_r Q$ and α are all variable parameters (see section 5.1.2).

[41] From the P and S wave velocity profiles we calculate a set of traveltimes, which in the present case is done using a standard ray theoretical approach. As for the body wave traveltime data set employed here, P and S wave traveltimes were obtained from the reprocessed ISC catalog [*Engdahl et al.*, 1998], covering epicentral distances of 18.5–90° for P waves and 19.5–80° for S waves, corresponding to depths of around 2500 km.

4.3. Solving the Forward Problem III: Mass and Moment of Inertia

[42] Mean mass and moment of inertia are obtained by simple integration of the estimated bulk density profile

$$I = \frac{8\pi}{3}\int \rho(r) r^4 dr, \qquad M = 4\pi \int \rho(r) r^2 dr \tag{8}$$

Values adopted for Earth's average mass (M) and moment of inertia (I) are $5.9733 \pm 0.009 \times 10^{24}$ kg and $0.33069 \pm 0.000009\ I/MR^2$, respectively, where R is the mean radius of the Earth (6371 km) [*Chambat and Valette*, 2001].

5. Solving the Inverse Problem

5.1. Parameterization of the Model

[43] We assume a spherically symmetric model of the Earth divided into four concentric shells of variable thickness, corresponding to crust, upper mantle, lower mantle and core. Crust and mantle shells are described by the model parameters thickness d, composition c and temperature T, whereas the physical properties of the core are specified by its radius, density. The simplification for the core layer was made because of a lack of thermodynamic data required to model metallic compositions. To determine the mineralogical structure and corresponding mass density it is also necessary to specify the pressure profile. For this purpose the pressure is obtained by integrating the load from the surface (boundary condition $p = 10^5$ Pa). In the following subsections the parameters and their prior distributions are described.

5.1.1. Mantle Composition

[44] The crust and mantle are parameterized by the composition c in the chemical system CaO-FeO-MgO-Al_2O_3-SiO_2. The oxide proportions of these elements are log-uniformly distributed within fixed intervals. In the upper mantle, the ranges are CaO $\in$ [2.3; 3.9], FeO $\in$ [7.2; 8.8], MgO $\in$ [34; 41.6], $Al_2O_3 \in$ [2.9; 4.9] and $SiO_2 \in$ [40; 49] (all in wt-%), in accordance with the range in upper mantle estimates of various workers [see *Lyubetskaya and Korenaga*, 2007, Table 2]. For the lower mantle we have, CaO $\in$ [2.5; 4.5], FeO $\in$ [5; 15], MgO $\in$ [33; 45], $Al_2O_3 \in$ [3; 6] and $SiO_2 \in$ [40; 55]. In each layer the normalization constraint $\Sigma_i c_i = 100$ wt% applies. Given the insensitivity of the traveltime data to the crustal structure, we used the average crustal velocity profile for continents determined by *Mooney et al.* [1998].

5.1.2. Temperature

[45] T in any given layer is distributed uniformly within the temperatures in the layers ultimately above and below, i.e., the temperature in layer k is determined from $T_k = T_{k-1} + \alpha \cdot (T_{k+1} - T_{k-1})$, where α is a uniformly distributed random number in the interval [0; 1]. A mantle adiabat for a potential temperature of approximately 1200°C, computed from a thermodynamic model assuming a pyrolitic bulk composition [*Ringwood*, 1975], was used as a lower bound on nodal temperatures, while no upper bound is applied. Surface temperature is held constant at 0°C. Temperatures are subsequently evaluated at 40 nodes at intervals of 50 km in the depth range 0–1000 km and were increased to 200 km in the depth range from 1000 km down to the core-mantle boundary (CMB).

5.1.3. Layer Thickness

[46] The crust and mantle layers are of variable thickness d and assumed to be uniformly distributed within the intervals $d_{cr} \in$ [5; 35] km, $d_{UM} \in [d_{cr}$; 1500 km], where d_{UM} is the thickness of the upper mantle layer. The thickness of the lower mantle is thus constrained to lie in the interval $d_{LM} \in [d_{UM}; r_s - r_{oc}]$, where r_s is radius of the Earth and r_{oc} is outer core radius, the latter two anchored at 6371 km and 3480 km (PREM), respectively.

[47] The thermodynamic models are used to establish the mineralogy, density and physical properties within the silicate layers at 40 depth nodes (same parameterization as for T) from the surface downward as a function of pressure, temperature and composition.

5.1.4. Attenuation

[48] To calculate a radial shear attenuation profile using the approach outlined in section 4.2, we assume that Q_0 and $\nabla_r Q$ are uniformly distributed within the intervals [50; 100] and [−0.1; 1.0], respectively, assuring that $Q(r)$ can either decrease, remain constant or increase as a function of depth. For the frequency exponent α in equation (7), we chose an uniform distribution within the interval 0.1–0.4, in line with recent measurements by *Jackson et al.* [2002] as well as theoretical expectations by *Minster and Anderson* [1981].

5.1.5. Core Physical Properties

[49] The core is parameterized by outer and inner core radii r_{oc}, r_{ic}, where r_{ic} is fixed at 5150 km depth in accordance with PREM, and corresponding variable densities (ρ_{oc}, ρ_{ic}). The latter parameters are distributed uniformly in the intervals, $\rho_{oc} \in [\rho_m; \rho_c]$ and $\rho_{ic} \in [\rho_{oc}; \rho_c]$ where ρ_m ρ_m is the value of ρ at the base of the mantle, as determined from thermodynamic modeling, and $\rho_c = 13$ g/cm^3.

[50] In summary, our model parameter vector is given by $\mathbf{m} = \{c_{ij}, T_l, d_k, \rho_{oc}, \rho_{ic}, Q_0, \nabla_r Q, \alpha\}$, consisting of 53 parameters.

5.2. Sampling the Posterior Distribution

[51] According to equation (2) the prior pdf $\eta(\mathbf{m})$ is modified by taking into account information provided by data and physical laws, contained in the likelihood function $\mathcal{L}(\mathbf{m})$, to yield the posterior pdf. Assuming that data noise can be modeled using a gaussian distribution and that observational uncertainties and calculation errors are inde-

Table 3. Two Mantle Compositions, Drawn From the Posterior Distribution, for Which Phase Equilibrium Diagrams are Shown[a]

	CaO	FeO	MgO	Al_2O_3	SiO_2
Model 1					
Upper mantle	2.3	8.5	38.6	2.9	47.6
Lower mantle	4.2	12.9	36.9	4.7	41.3
Model 2					
Upper mantle	2.4	7.9	39	2.9	47.7
Lower mantle	3.1	14.5	37.6	3.2	41.7

[a] See Figure 1. All numbers in wt%.

pendent among the different geophysical methods employed, the likelihood function can be written as

$$\mathcal{L}(\mathbf{m}) \propto \exp\left(-\sum_i \frac{\left[d^{P^i}_{obs} - d^{P^i}_{cal}(\mathbf{m})\right]^2}{2\varepsilon_i^2} - \sum_j \frac{\left[d^{S^j}_{obs} - d^{S^j}_{cal}(\mathbf{m})\right]^2}{2\varepsilon_j^2} - \frac{\left[d^{M}_{obs} - d^{M}_{cal}(\mathbf{m})\right]^2}{2\varepsilon_M^2} - \frac{\left[d^{I}_{obs} - d^{I}_{cal}(\mathbf{m})\right]^2}{2\varepsilon_I^2} \right) \tag{9}$$

where d_{obs} denotes observed data, with superscripts alluding to the particular geophysical observation, $d_{cal}(\mathbf{m})$ calculated data and ε the uncertainty on either of these.

[52] To sample the posterior distribution using the Metropolis-Hastings algorithm outlined in section 3.2, we adopt the following strategy: in each iteration a shell j was chosen at random and subsequently all parameters pertaining to this shell were perturbed using the proposal (= prior) distribution as defined in the previous section. Next we calculated "synthetic" data and computed the acceptance probability for the perturbed model parameter vector $\mathbf{m}'$ as min[1, $\mathcal{L}(\mathbf{m}')/\mathcal{L}(\mathbf{m})$]. The adopted proposal distribution has a burn-in time of $\sim 10^4$ iterations after which we started retaining samples. To ensure convergence of the MCMC algorithm, we monitored the time series of all output parameters from the algorithm to verify that these were indeed stationary over the many iterations performed. The question as to how many samples are needed to adequately represent the posterior pdf, is assumed answered once there are no longer any significant changes to the characteristics of the posterior pdf. To obtain independent samples, we introduced an "elapse time" (number of iterations) between retention of samples, which was found to be around 100 by analyzing the autocorrelation function of the fluctuations of the likelihood function. In all 10^7 models were sampled with an overall acceptance rate of 34%.

[53] The solution to the inverse problem is a pdf, which, owing to the strongly nonlinear character of the problem, is complex (typically multimodal), and single measures such as means, medians or maximum likelihood models are generally inadequate descriptors. We adopt the approach of *Tarantola* [2004], who advocates the direct examination of the prior and posterior pdf's, as a means of gaining insight into which parameters and model features are resolved. In the following prior and posterior pdf's are displayed next to each other as a simple means of measuring the amount of information contained in the data. If the posterior pdf has changed shape, has narrowed or been displaced relative to the prior, it signifies that data can constrain that particular parameter. We will not necessarily be drawing the attention of the reader to this, but encourage the reader to keep it in mind when scrutinizing the results.

6. Results and Discussion

6.1. Phase Equilibria

[54] Nine phases are stable in the upper mantle and transition zone in our system. These are anorthite (An), spinel (Sp), olivine (Ol), orthopyroxene (Opx), clinopyroxene (Cpx), the high-pressure polymorph of Mg-rich Opx of C2/c symmetry (C2/c), garnet (Gt), wadsleyite (Wad) and ringwoodite (Ring). The lower mantle comprises the phases magnesiowüstite (Wus), akimotoite (Aki), perovskite (Pv), calcium-perovskite (Ca-pv) and postperovskite (Ppv). We calculated phase equilibria using several different pyrolite compositions and geotherms and compared these with available experimental data by [*Irifune and Isshiki*, 1998] as well as the phase equilibria calculated by *Stixrude and Lithgow-Bertelloni* [2005a, 2007] for the upper mantle and transition zone. Our calculated phase diagrams (not shown) were found to be in good agreement with both. In our earlier work [*Khan et al.*, 2006a, 2006b, 2006c; *Khan and Connolly*, 2008], we have emphasized the importance of considering phase equilibria in geophysical applications where physical properties (e.g., density, seismic wave velocities, electrical conductivities) are employed to estimate geophysical data, which need to be compared to observations. These studies showed that changes in phase equilibria induced through compositional and thermal variations are significant, because the different minerals have different physical properties, which, when combined with different model proportions can lead to significant changes in bulk physical properties and thus geophysical responses. As a quantitative example we illustrate this by investigating the differences in geophysical responses that arise as a consequence of considering small variations in composition and temperature.

[55] We consider the two compositions given in Table 3 that are drawn randomly from the sampled posterior distribution (as are their corresponding geotherms), i.e., both models fit data within uncertainties. The calculated phase equilibria for the two compositions and their geotherms are shown in Figure 1. The similarity in composition and geotherm result in essentially similar upper mantle phase equilibria. While lower mantle transitions in the two models occur at almost equal pressure, 23.55 and 23.51 GPa, respectively, phase equilibria in the transition zone and lower mantle differ somewhat. This is due mostly to the use of slightly different thermal profiles, given that only CaO, FeO and Al_2O_3 contents vary, with little influence on lower mantle mineralogy. The main determining factor with regard to lower mantle mineralogy is the Mg/Si ratio, which determines the abundance of Pv and Wus. Other differences occur in the lowermost mantle, with Ppv being stabilized at lower pressure in model 2 (Figure 1f) because of lower temperatures. In addition to this, bulk physical properties (ρ, V_P, V_S) calculated on the basis of the equilibrium mineralogies are shown in Figure 2. We have indicated locations of phase changes (letters a to g in Figures 2a–2c) that give rise to more or less prominent discontinuities in all physical properties. Interpreting these transitions is most easily done by comparison with Figure 1, where, as an example, we also

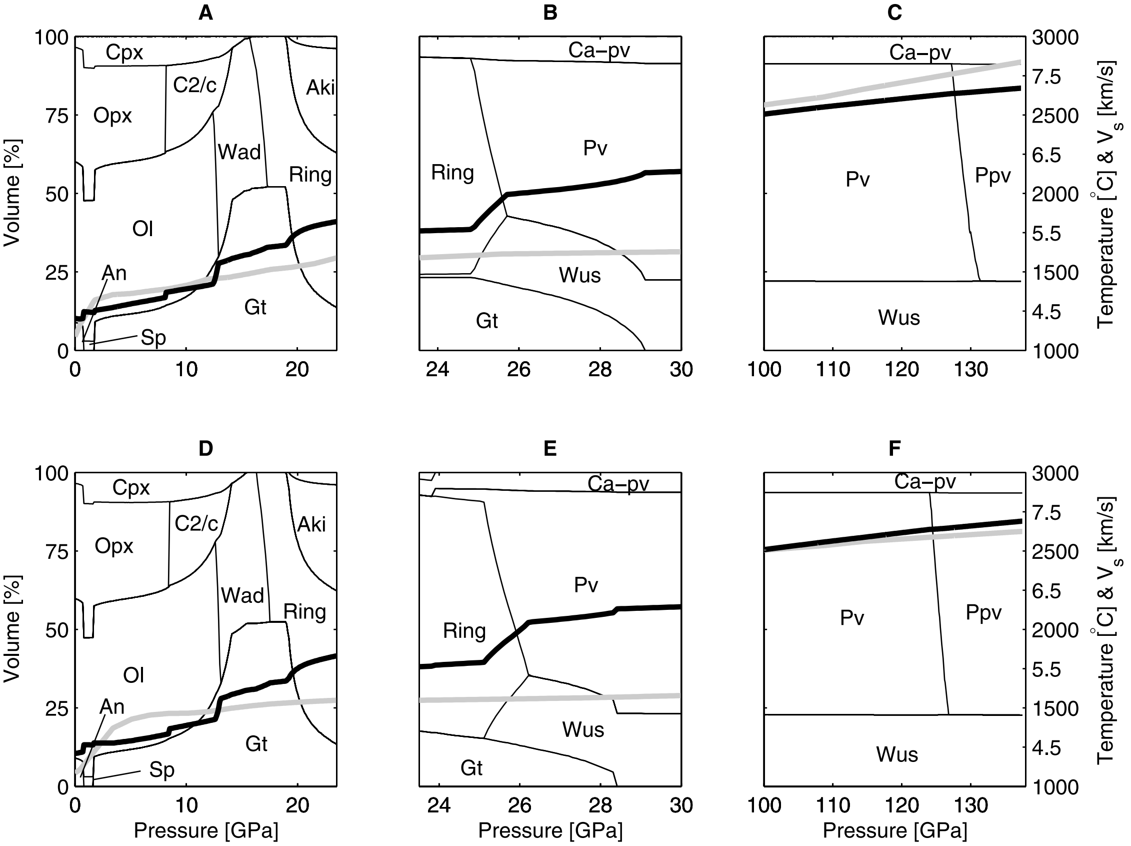

Figure 1. Examples of equilibrium mineralogies estimated using our self-consistent phase equilibrium calculation for two model compositions and geotherms (gray lines) drawn from the posterior distribution. Modal mineralogy for model 1 (a–c) and model 2 (d–f). The solid black line is the *S* wave velocity profile calculated for the two models. Note that the y axis to the right of Figures 1c and 1f contains both temperatures (gray line) and *S* wave velocities (black line). Also, note that only the bottom part of the lower mantle is shown. The model compositions are tabulated in Table 3.

show the change in *S* wave velocity accompanying a given phase transformation by superposing V_S as a function of pressure on the equilibrium phase diagram plots for both models (Figure 1, black line). The transition labeled a (see Figure 2a) is seen to be due to the transformation of Cpx to C2/c, whereas b indicates the transformation of Ol to Wad, which coincides with the 410 seismic discontinuity, while c reflects the transformation of Wad to Ring, possibly indicative of the 520 seismic discontinuity, and d reflects the appearance of Aki. Other major discontinuities include those labeled e and f, where transition e (Figure 2b), which is a result of the transformation of Ring to Pv + Wus, indicates the boundary between upper and lower mantle (the 660 seismic discontinuity), while f occurs as all Gt is being transformed to Pv. Finally, transition g marks the base of the lower mantle (D″) as Pv transforms to Ppv. While differences in physical properties between the two models are very subtle in the upper mantle, differences are discernable in the transition zone and the lower mantle. In particular, between the two models, the "660" discontinuity is seen not only to occur at slightly different pressure (depth), but it also shows distinct physical features. In model 1, the "660" is more drawn out and varies more smoothly than in model 2. The latter is characterized by having a small secondary jump at ~28.5 GPa, following the main discontinuity at ~25 GPa, not observed in model 1. This additional feature in model 2 is related to a more abrupt disappearance of Gt, whereas in model 1, Gt changes in a continuous fashion until all of if it has been transformed, producing a more smooth transition below the main jump. In the lowermost mantle, the Pv→Ppv transition occurs at somewhat lower pressure in model 2 than in model 1, due principally to lower mantle temperatures in the former. This is clearly reflected in all physical properties (Figures 2c, 2f, and 2i). Although the overall differences between the two models might seem small, they do result in significantly different traveltime fits.

6.2. Calculated Data

[56] Comparison of the calculated and observed geodetic (Figure 3) and seismic (Figure 4) data shows that we fit these within the corresponding uncertainties. In relation to this, it is particularly satisfying that the most probable *P* and *S* wave traveltime fits are centered around 0 s and well within the observational uncertainties. These fits show little structure, except for maybe at epicentral distances <25°, an effect attributed to the dearth of constraints provided by the traveltime data at these distances (corresponding to the upper 300 km depth). In comparison, *Cammarano et al.*

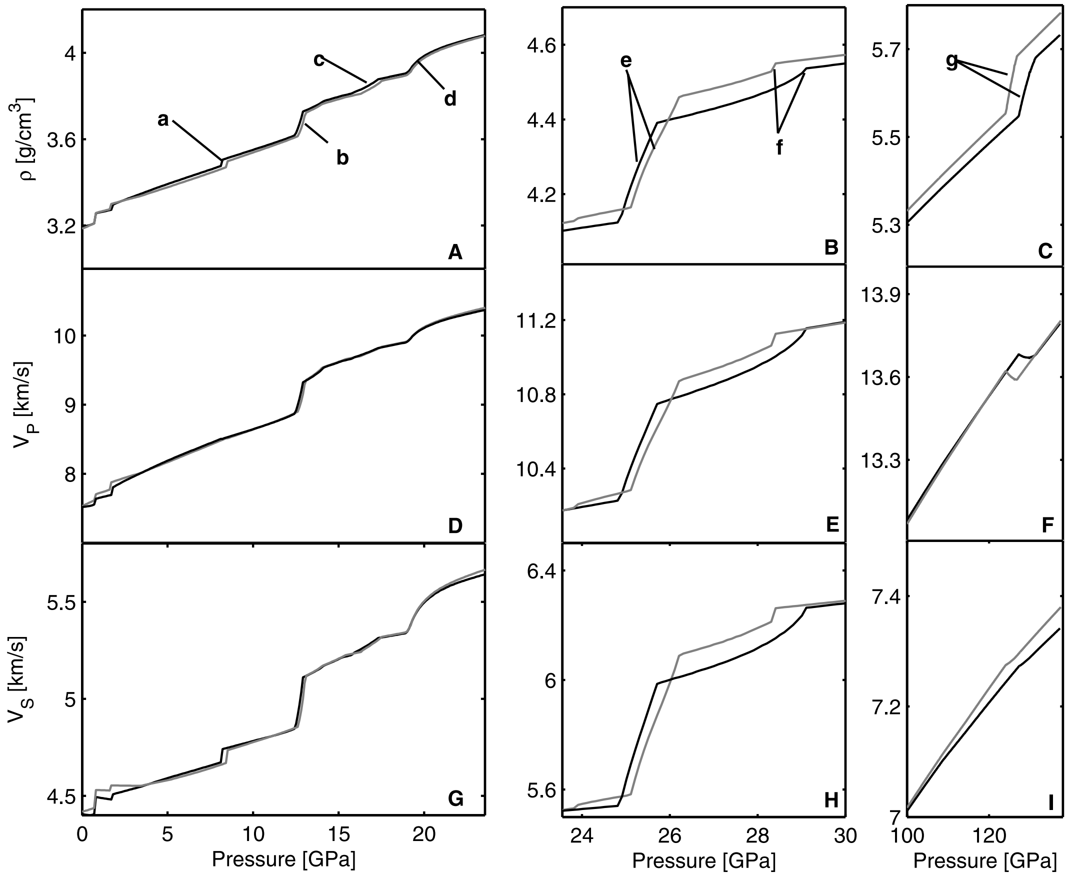

Figure 2. Physical properties for the two equilibrium mineralogies shown in Figure 1. Black line is for model 1, and gray line denotes model 2. The figures are arranged so that top is density (a–c), middle is *P* wave velocity (d–f), and bottom is *S* wave velocity (g–i). (left) Upper mantle, (middle) transition zone, and (right) lower mantle. Lowercase letters (a–g) in Figures 2a–2c indicate locations of major phase transitions observed in the phase equilibrium plots. See main text for further discussion.

[2005], who considered the same traveltime data set, obtained traveltime fits with prominent structure, and had problems fitting data (their Figures 4 and 6), which most probably stems from constraining the composition to pyrolite as well as being limited to an adiabatic geotherm. On the traveltime difference curves is also shown the fit to the observations calculated on the basis of PREM. Our fits are systematically better than those calculated using PREM, especially in the case of *S* waves, which is most probably related to PREM being based on a combination of short (traveltimes) and long-period (surface waves, normal modes) data sets. Given that we constrain crustal velocities to an average profile over continents, a continental bias is likely introduced in the results. However, this bias is to a certain extent already reflected in the traveltime data set given the greater number of stations over continents.

6.3. Upper Mantle Composition

[57] Upper mantle compositions are shown in Figure 5. We have also included some literature estimates for the composition of the Earth's primitive upper mantle (PUM) composition (the composition of the mantle prior to extraction of basaltic crust, but postdating core formation) by *McDonough and Sun* [1995] and a very recent estimate by *Lyubetskaya and Korenaga* [2007]. These estimates rely on one of two approaches that is employed in deriving the composition of the PUM of the Earth. In the cosmochemical approach interelement relationships derived from meteorites, principally CI carbonaceous chondrites (taken as rep-

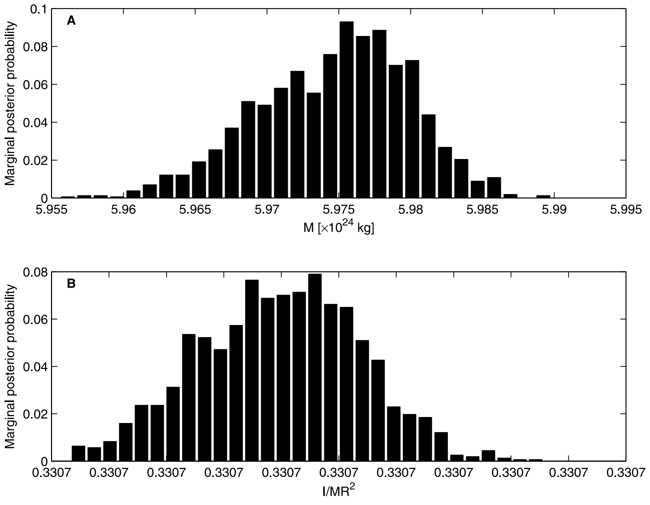

Figure 3. Marginal posterior geodetic data distributions. (a) Mass (M_{obs} = 5.9733 ± 0.009) and (b) moment of inertia (I_{obs} = 0.33069 ± 0.00001).

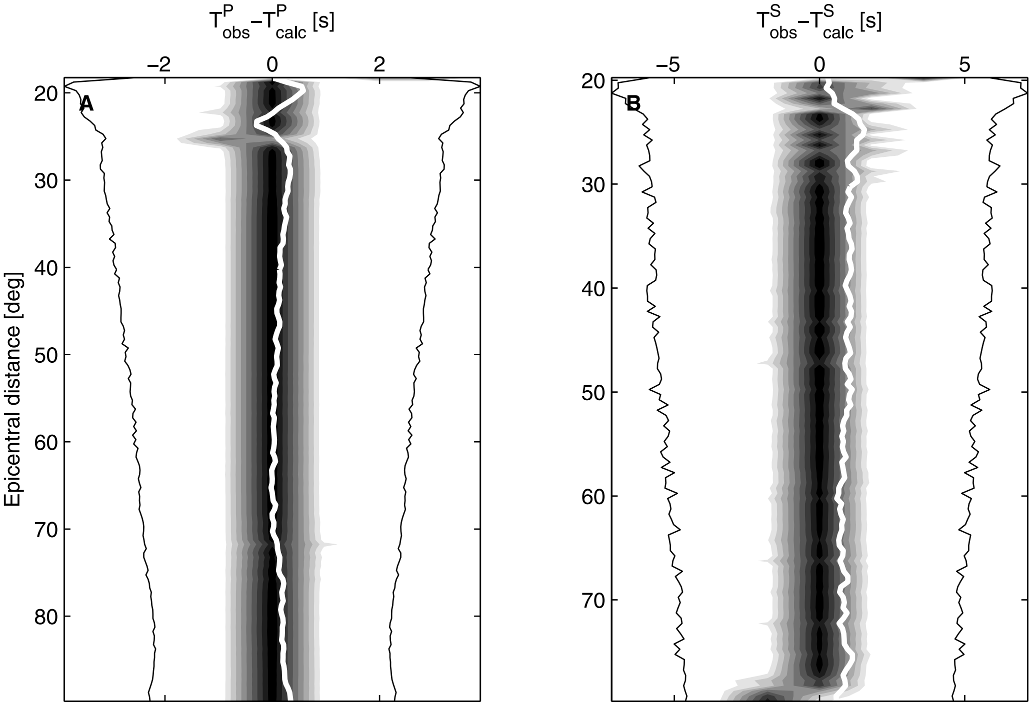

Figure 4. Marginal posterior traveltime data distributions as a function of epicentral distance, shown as traveltime differences, i.e., observed less calculated. (a) *P* wave traveltimes differences and (b) *S* wave traveltimes differences. Shades of gray indicate probability of occurrence of a given value of traveltime difference, with color coding as follows: (white) least to (black) most probable. Black lines denote uncertainties, and white lines denote traveltimes differences calculated on the basis of Preliminary Reference Earth Model (PREM).

resentative of the primitive solar nebula rock fraction on account of their match to solar photosphere abundances for the nonvolatile elements) are employed [e.g., *Taylor*, 1980; *Palme and O'Neill*, 2003]. The geochemical avenue, on the other hand, uses the data from mantle xenoliths and basalts erupted from the mantle [e.g., *Jagoutz et al.*, 1979; *McDonough and Sun*, 1995; *McDonough and Rudnick*, 1998; *Lyubetskaya and Korenaga*, 2007]. A basic but reasonably robust assumption in the cosmochemical approach is that the ratios among the refractory lithophile elements (RLE) in the Earth are similar to those in the CI chondrites. The only relevant terrestrial samples available for our inspection are basalts and xenoliths derived from the upper mantle. The latter sample only the upper few hundred km of the 2900 km thick mantle while they are also subject to metasomatic alteration.

[58] Currently there are two differing interpretations of the meteorite and xenolith database. The most widely quoted are the "standard" estimates of *McDonough and Sun* [1995] and *Palme and O'Neill* [2003]. The most recent geochemical estimate of *Lyubetskaya and Korenaga* [2007] employ much the same data investigated by McDonough and Sun, while the earlier cosmochemical study by *Taylor* [1979, 1980] is akin to that of Palme and O'Neill. The studies by *Taylor* [1979, 1980] and Lyubetskaya and Korenaga disagree to some extent with the standard values, with the most significant differences between the two sets in our context occurring for Al and Ca. Table 4 as well as Figure 5 show that CaO and Al_2O_3 are significantly depleted in the estimates by Taylor and Lyubetskaya and Korenaga in comparison to those of McDonough and Sun and Palme and O'Neill, while FeO, MgO and SiO_2 contents are the same within the uncertainties. Our purely geophysically derived estimates for the composition of the PUM seem to reinforce the results by Lyubetskaya and Korenaga and Taylor, with most probable CaO and Al_2O_3 contents of $\sim$2.4 and $\sim$3 wt%, respectively (see Figures 5a and 5d). In addition, the pdf's indicate overall lower CaO and Al_2O_3 contents than implied by, e.g., McDonough and Sun. FeO, MgO and SiO_2 are found to be within uncertainties of earlier estimates. Sampled Mg#'s of 0.89 are found, in general agreement with most estimates, whether geochemically or cosmochemically derived. Mg/Si wt ratios around 1.05 are obtained, which is a bit lower than the "standard" values, but nonetheless are in agreement to within their uncertainties. It has not escaped our attention that discrepancies of major geophysical importance occur for the remaining refractory lithophile elements (RLE, including U and Th) and the abundance of potassium and other volatile elements. These include the terrestrial argon budget, the potassium abundance of 180 ppm rather that 260 ppm, the mass balance of the RLE elements (2.16–2.23 × CI [*Lyubetskaya and Korenaga* [2007]; *Taylor*, 1980] compared to 2.5–2.8 × CI [*Jagoutz et al.*, 1979; *Hart and Zindler*, 1986; *McDonough and Sun*, 1995; *Palme and O'Neill*, 2003]), and the global thermal budget (for a recent discussion, see *Korenaga* [2008]).

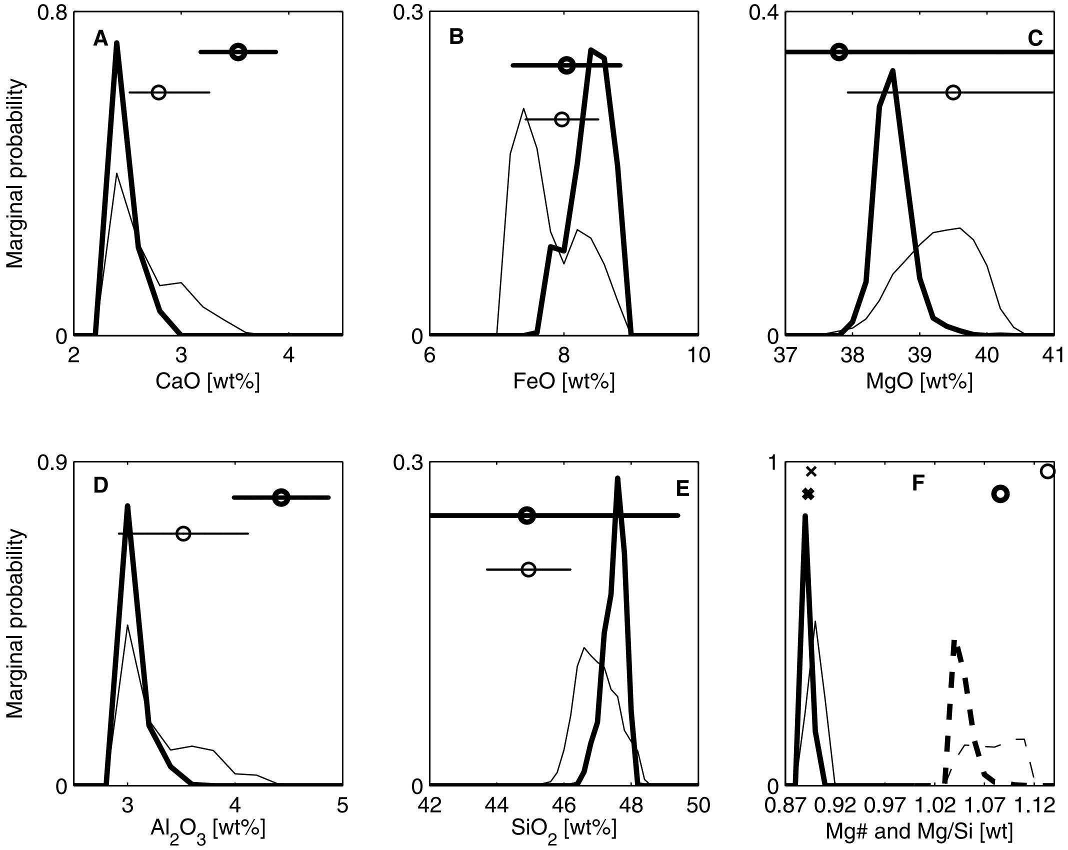

Figure 5. Marginal prior (thin line) and posterior (thick line) probability distributions showing sampled upper mantle compositions. (a–e) CaO-FeO-MgO-Al$_2$O$_3$-SiO$_2$ (CFMAS) oxide contents and (F) Mg# (solid line) and Mg/Si ratios (dashed line). In Figures 5a–5f, circles, crosses, and bars indicate the compositions and uncertainties of the primitive upper mantle of *McDonough and Sun* [1995] (heavy), and *Lyubetskaya and Korenaga* [2007] (thin). The prior distributions are skewed because these are plotted in wt% rather than using the logarithm.

6.4. Lower Mantle Composition

[59] As there are no terrestrial samples from the lower mantle, a traditional assumption is to invoke a chemically homogeneous mantle, i.e., that the upper mantle composition is representative of the entire mantle, or equivalently, that basalt petrogenesis is the sole responsible for changing the major element chemistry of geochemically significant portions of the mantle. Basalt petrogenesis, the basis of Ringwood's pyrolite model [e.g., *Ringwood*, 1975], has resulted in a number of mantle compositions [e.g., *Allégre et al.*, 1995; *McDonough and Sun*, 1995; *Salters and Stracke*, 2004] that are in close accord with one another. The question as to whether these compositions, which have been determined with a precision between 1% [*Palme and O'Neill*, 2003] and 10% [*McDonough and Sun*, 1995] (see Table 4) are indeed representative of the composition of the silicate Earth is an as yet unresolved question.

[60] In a first attempt to answer this question, we asked whether it is possible to fit the geophysical data investigated here under the assumption that (1) the mantle be chemically homogeneous and that its composition lies somewhere within the uncertainties of earlier estimates (see section 5.1.1 for the prior pdf on upper mantle composition), and (2) a variable geotherm, which can be either subadiabatic, superadiabatic,

Table 4. Present (Most Probable Values) and Some Previous Estimates of the Earth's Primitive Upper Mantle Composition and Their Uncertainties[a]

Study	CaO	FeO	MgO	Al$_2$O$_3$	SiO$_2$
Lyubetskaya and Korenaga [2007]	2.79 ± 0.47	7.97 ± 0.54	39.5 ± 1.53	3.52 ± 0.6	44.95 ± 1.24
McDonough and Sun [1995]	3.53 ± 0.35	8.04 ± 0.8	37.8 ± 3.8	4.43 ± 0.44	44.9 ± 4.5
Palme and O'Neill [2003]	3.66 ± 0.037	8.12 ± 0.08	36.85 ± 0.37	4.51 ± 0.36	45.5 ± 0.46
Taylor [1980]	2.65	8	40	3.3	45
Upper mantle, this study	2.4	8.4	38.5	3	47.5
Lower mantle, this study	2.8	13.5	38	3.3	42

[a] Note that no uncertainties are indicated for the values found here. For these the reader is referred to the posterior probability distributions (Figures 5 and 6).

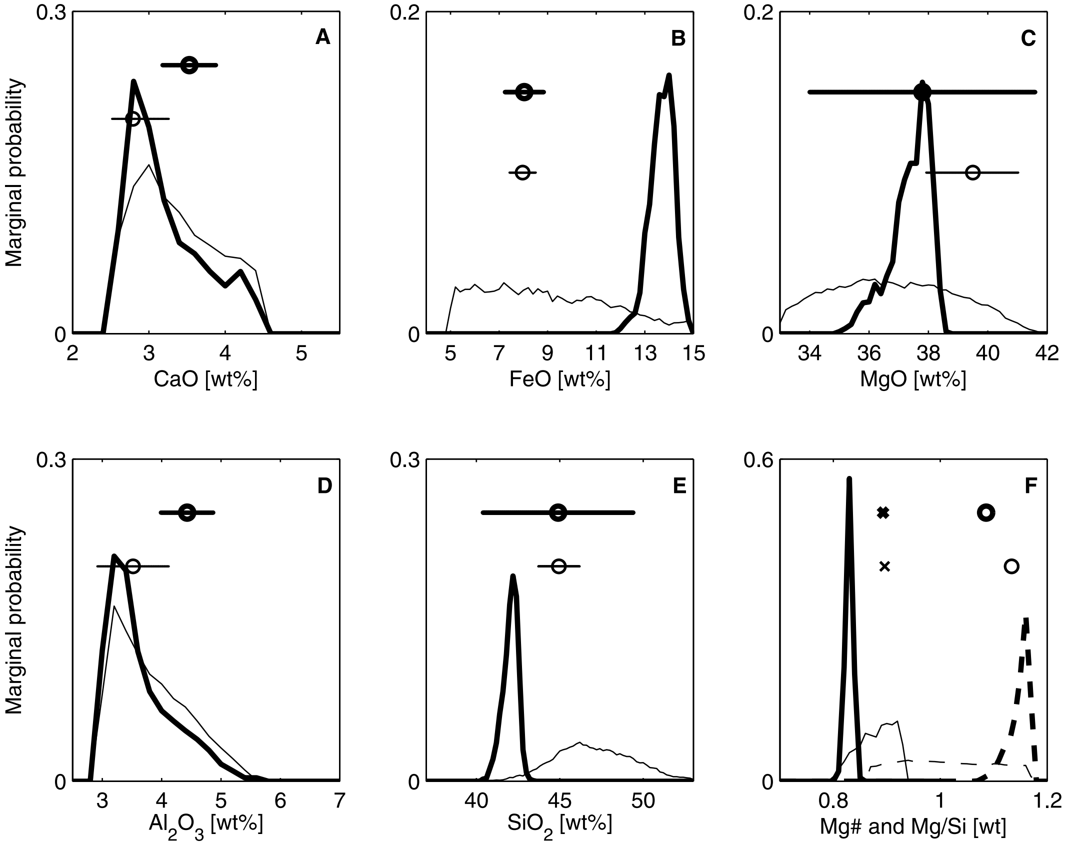

Figure 6. Marginal prior (thin line) and posterior (thick line) probability distributions showing sampled lower mantle compositions. (a–e) CFMAS oxide contents and (F) Mg# (solid line) and Mg/Si ratios (dashed line). In Figures 6a–6f, circles, crosses, and bars indicate the compositions and uncertainties of the primitive upper mantle of *McDonough and Sun* [1995] (heavy), and *Lyubetskaya and Korenaga* [2007] (thin). The prior distributions are skewed because these are plotted in wt% rather than using the logarithm.

or simply adiabatic. We found this not to be possible for any configuration of composition and geotherm, concluding that a chemically homogeneous pyrolite mantle is not compatible with present geophysical data. Having obtained this result, we went on to investigate which lower mantle composition then is line with the geophysical data, prior information (section 5.1) and the physical laws relating unknown model parameters to data (section 4).

[61] The lower mantle compositions are shown in Figure 6 where prior pdf's are, as in the case of the upper mantle, significantly narrowed in comparison to posterior pdf's, implying that data are able to provide constraints on the Earth's lower mantle composition. Upper mantle estimates of *McDonough and Sun* [1995] and *Lyubetskaya and Korenaga* [2007] are superposed for comparison. The latter composition is also indicative of our PUM estimates. CaO and Al_2O_3 are slightly enriched relative to our upper mantle estimates (see Figure 5) and closely agree with Lyubetskaya and Korenaga. MgO is also within the uncertainties of our PUM estimates and previous models, with most probable values around 38 wt%. Differences arise for SiO_2 and especially for FeO, where we find most probable values of 42 and 13.5 wt%, respectively, implying FeO enrichment of the lower mantle relative to the upper mantle, as well as slight depletion of SiO_2, although it should be noted that this value is within the uncertainty of the SiO_2 content found by McDonough and Sun. The differences found here for FeO and SiO_2 result in a significantly lower Mg# of ~0.83–0.84 as well as a higher Mg/Si ratio of ~1.2, in comparison to ~0.89 and ~1.1 for PUM.

[62] The terrestrial planets are believed to have been derived from material emanating from a broad region of the inner solar system, implying significant radial mixing during planetary accretion, although modeling has shown that each planet generally accretes a higher proportion of more localized material [e.g., *Wetherill*, 1994; *Chambers*, 2001], and thus retains some form of compositional memory. While it is generally assumed that the Earth is derived from chondritic material, it has proven difficult to assemble the Earth from any known chondrite or even combinations thereof [e.g., *Burbine and O'Brien*, 2004], given the diversity in chemical compositions spanned by these [*Jarosewich*, 1990]. This is best exemplified in the dilemma of Mg/Si estimates from xenolith data, as the latter consistently indicate that the upper mantle of the Earth has a high Mg/Si ratio (~1.1) compared to the CI meteorites (~1). Is this ratio typical of the whole mantle or only the upper part accessible to sampling? Mg and Si are not included among the refractory lithophile elements and many of the chondritic meteorite groups show differences in Mg/Si ratios from the

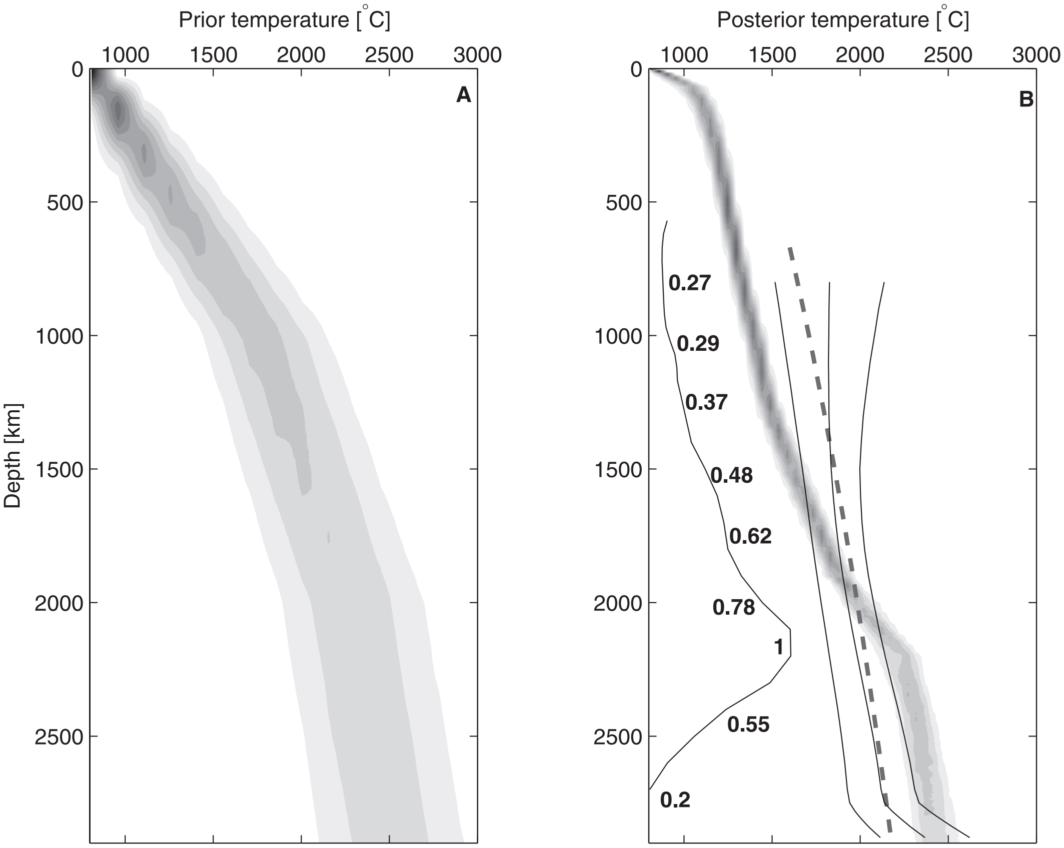

Figure 7. Marginal prior (a) and posterior (b) pdf's showing sampled geotherms as a function of depth. Thin black lines indicate the average temperatures and uncertainties on model DT2 [*Deschamps and Trampert*, 2004]. Dashed line is the profile determined by *Brown and Shankland* [1981], and the thin line with numbers shows the geothermal gradient as a function of depth determined here, with numbers indicating the value of the geothermal gradient in °C/km at the particular location. Shades of gray as before.

CI values, indicative of fractionation of these elements in the inner nebula. Interestingly the refractory elements Ca and Al also have higher ratios in upper mantle xenoliths (1.3) than in CI (1.1), although melting during magma production is usually blamed for this discrepancy [*Palme and Nickel*, 1985]. Possible solutions to the conundrum of the high Mg/Si ratio relative to CI have been to either (1) invoke other building blocks, ranging from the EH enstatite chondrite family [*Javoy*, 1995; *Lodders*, 2000] over the EL chondrites [*Burbine and O'Brien*, 2004] to an "Earth chondrite" or "Earth achondrite" (matching the Earth's oxygen isotopic composition and Mg/Si and Al/Si ratios of the primitive upper mantle), which either no longer exists or as yet remains unsampled [*Drake and Righter*, 2002], or (2) to argue that samples from the upper mantle are not representative of the entire mantle, leading to the possibility of constructing the Earth from cosmic abundances, resulting in a mantle that is neither homogeneous nor primordial [e.g., *Anderson*, 2002], or as a variant thereof, (3) to suggest that it is balanced by a lower Mg/Si in the lower mantle or that the missing Si is in the core, so that the Earth has the Mg/Si ratio of the primitive solar nebula [*Allégre et al.*, 1995]. However, the wide variation in the observed Mg/Si ratio among meteorites does not encourage such suggestions, for the Earth most probably assembled from a hierarchy of (often differentiated) planetesimals. Although the highly reduced enstatite chondrites are considered as possible candidates, because they share the same oxygen isotopic composition as the Earth [*Javoy*, 1995], their low Al/Si and Mg/Si ratios and their high K/U ratios rule them out. A current geochemical view, summarized by *Drake and Righter* [2002], holds instead that the mantle is likely uniform and that the terrestrial high Mg/Si ratios were derived from unsampled planetesimals. The lower mantle compositions derived here, with SiO_2 contents of 40–44 wt%, effectively rule out the lower mantle as a sink for any Si, leaving the core as only other possibility. *Burbine and O'Brien* [2004] estimated that if all the Si lost from the Earth's upper mantle had been sequestered into the core, this would amount to a core Si content of ~17 wt%, far in excess of allowed values, as the Earth's core is assumed to contain no more than ~10 wt% of a light alloying element [*Jeanloz*, 1990; *Poirier*, 1994]. A recent estimate by *Wood et al.* [2006] has the core containing at most 4–5 wt% of low-mass elements, rendering the core as explanation for the depleted Si as even more remotely possible. On this basis, it seems to be relatively safe to conclude that the bulk Earth silicate composition has a higher Mg/Si ratio than CI and that all the common

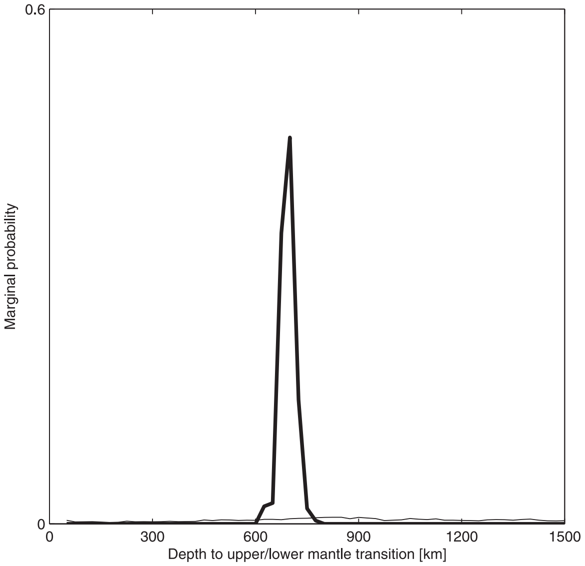

Figure 8. Marginal prior (thin line) and posterior (thick line) probability distributions depicting sampled upper mantle thickness or equivalently, depth at which a transition (chemical) occurs.

chondrites, which have lower Mg/Si ratios, do not match this composition.

[63] The lower mantle appears to differ in composition from that of the upper mantle; it is significantly enriched in FeO, which is balanced by a lower SiO_2 abundance than in the upper mantle, and therefore does not act as a sink for Si as often postulated. These findings present considerable petrological difficulties that will be addressed in a subsequent paper, but a few speculations may be made here. These element abundances do not follow the pattern expected from early differentiation nor do these differences appear to be due to the lower mantle being enriched from preferential accumulation of the subducting slabs. These should enrich the lower mantle in Si, not the reverse, so we judge that such an explanation is unlikely. The enrichment in FeO can account for much of the depletion in Si, but not the concomitant enrichment in Ca and Al. *Palme et al.* [2003] have noted that the bulk Earth Fe/Mg ratio is at least 10% higher than the Fe/Mg ratio of the average solar system (CI). Presuming that the Earth had differentiated, they suggest that early large impacts could have collisionally eroded silicate material from the mantle leaving it with an excess in Fe.

[64] For the sake of completeness, we would like to note that calculations were also made with a more recent thermodynamic formulation and parameterization for mantle phases proposed by *Stixrude and Lithgow-Bertelloni* [2005b, 2007]; however the quality of the resulting data fit was lower, and the lower mantle compositions were notably more calcic and aluminous (with CaO and Al_2O_3 contents in the range 7–8 wt%), than the results reported here.

6.5. Mantle Geotherm, Thermal Boundary Layer and Mantle Discontinuity

[65] The sampled prior and posterior mantle geotherms are shown in Figure 7. The Ol → Wad and Ring → Mw + Pv phase transitions, thought to explain the 410 and 660 km seismic discontinuities, are located at temperatures of 1230 ± 52°C and 1320 ± 45°C, respectively. These values are somewhat lower when compared to temperatures measured experimentally for the above reactions by *Ito and Takahashi*, [1989], who found of 1477 ± 100°C and 1577 ± 100°C, respectively. Down to about 1200 km depth our temperatures roughly follow an adiabat, when compared with the thermal profile of *Brown and Shankland* [1981] (dashed line in Figure 7b). This profile is almost adiabatic over the entire lower mantle, and was obtained from thermodynamic parameters calculated on the basis of seismic profiles. At about 1400 km depth our profiles depart from conditions of adiabaticity, with temperatures increasing to ~2300°C at a depth of 2100 km, and reaching ~2500°C in the bottom of the mantle. The temperatures found here at the CMB are below the solidus, estimated to be in excess of 4000°C, which is based on extrapolation of silicate perovskite and magnesiowüstite melting data to CMB conditions [*Zerr and Boehler*, 1993, 1994]. Also in Figure 7b is shown a thermal profile from the study by *Deschamps and Trampert* [2004] as well as their uncertainties. As summarized in Table 1, this geotherm was obtained from inversion of a 1D seismic profile (PREM) using EoS modeling and deviates slightly from the geotherm of Brown and Shankland for depths >1500 km.

[66] In Figure 7b are also indicated thermal gradients in the mantle, which are essentially superadiabatic from ~1300 km and down to a depth of about 2200 km. A thermal boundary layer (TBL) is clearly present in the mid to lower mantle (1800–2100 km depth) and as such concurs with inferences by *Deschamps and Trampert* [2004], who found, depending on modeling assumptions, evidence for at least a thin TBL at the bottom of the mantle.

[67] With regard to the TBL found here, it has not escaped our attention that it might possibly coincide with a chemical layer in the deeper parts of the lower mantle as proposed by *Kellogg et al.* [1999] and *Anderson* [2002, 2005]. Kellogg et al. suggested the presence of a deep global layer of primitive composition, with an average thickness of 1300 km, but varying by as much as ~1000 km, and constituting 30% of the mass of the Earth's mantle. What can be inferred from the present study about mantle discontinuities and chemical layering, as our results suggest a compositionally distinct upper and lower mantle?

[68] The parameter to be investigated is the variable thickness of the upper mantle, which a priori was uniformly distributed between the depth of the Moho and 1500 km depth (see section 5.1.3 for details). Sampled values for the thickness of the upper mantle are shown in Figure 8. The prior distribution is as expected flat, indicating that upper mantle thickness, or equivalently depth to upper/lower mantle transition, is to be found with equal probability between the depth of the Moho and 1500 km depth. The posterior pdf, meanwhile, is seen to be confined in the depth range 650–750 km, in addition to being strongly peaked at ~680 km depth. Taken at face value, this result is in line with interpretations of the seismic 660 km discontinuity as representing a change in chemistry on going from upper to lower mantle. We also looked for transitions deep in the lower mantle, i.e., at depths >1000 km, by running the algorithm with a fixed upper/lower mantle transition located

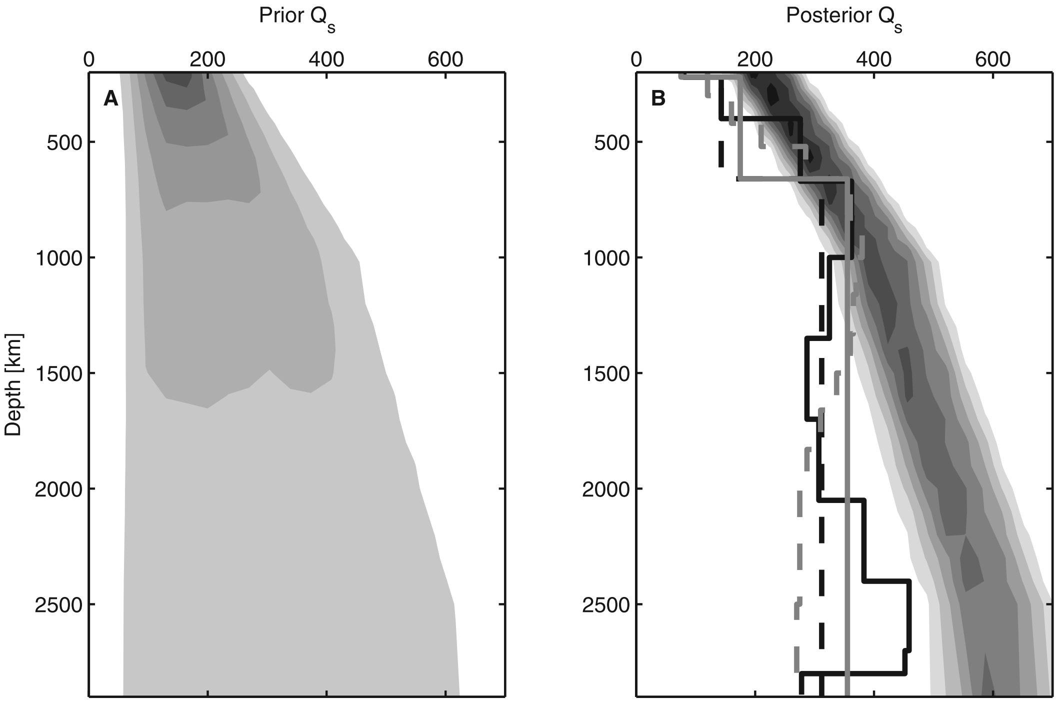

Figure 9. Marginal prior (a) and posterior (b) pdf's depicting radial shear attenuation profiles. Models derived from seismological studies are also shown for comparison. (black solid line) QLM9 [*Lawrence and Wysession*, 2006], (gray solid line) PREM, (black dashed line) QL6 [*Durek and Ekström*, 1996], and (dashed gray line) QM1 [*Widmer et al.*, 1991]. Shades of gray as before.

at 1200 km depth. Although this resulted in small changes in mantle composition and temperature, we did not achieve the required data fit, i.e., we were not able to fit all data within uncertainties. A preliminary analysis of the output from this inversion, showed little variation in physical properties (ρ, V_S and V_P) across the 1200 km discontinuity, which is most probably due to the increasing role of pressure in the lower mantle counteracting temperature effects. As a consequence of this canceling of effects, chemical discontinuities deep in the lower mantle will be less pronounced physically and therefore difficult to discern.

6.6. Physical Properties: Shear Attenuation

[69] Radial shear attenuation profiles are shown in Figure 9. Comparison of prior and posterior $Q_S(r)$ clearly indicates a significant change in the posterior pdf. The qualitative characteristics of seismically derived models for radial shear attenuation generally agree with ours (also shown in Figure 9) down to about ~1000 km depth, indicating an increase in Q_S throughout the upper mantle and into the upper part of the lower mantle. For depths >1000 km there is less agreement. Some of the earlier models decrease, while others remain constant, whereas our models are signified by an increase in Q_S throughout the lower mantle. Though not shown here, we would like to note that large Q_S values (400–600) in the lower mantle were also found by *Montagner and Kennett* [1996]. For the upper and lower mantle, weak frequency dependencies, in agreement with seismological [*Anderson and Given*, 1982] and experimental studies [*Jackson et al.*, 2002], are found, with values of α generally >0.3 (see Figure 10).

[70] While we have taken attenuation effects into account, it can be argued as done by *Deschamps and Trampert* [2004] and *Stacey and Davis* [2004] that extrapolating from laboratory measurements made at ~MHz frequencies down to seismic frequencies using equation (7) may not be appropriate, as it is not certain that the absorption band model is applicable over such a large frequency range. We investigated the effect of disregarding attenuation, by un-

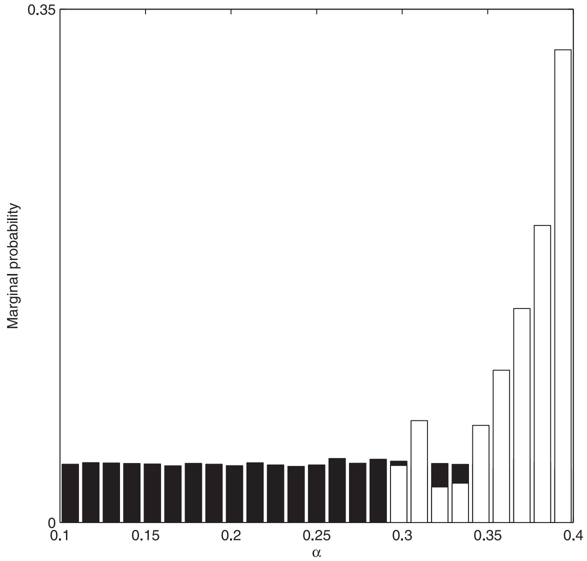

Figure 10. Marginal prior (black bars) and posterior (white bars) pdf's showing the values obtained for α, which expresses the frequency dependence of Q.

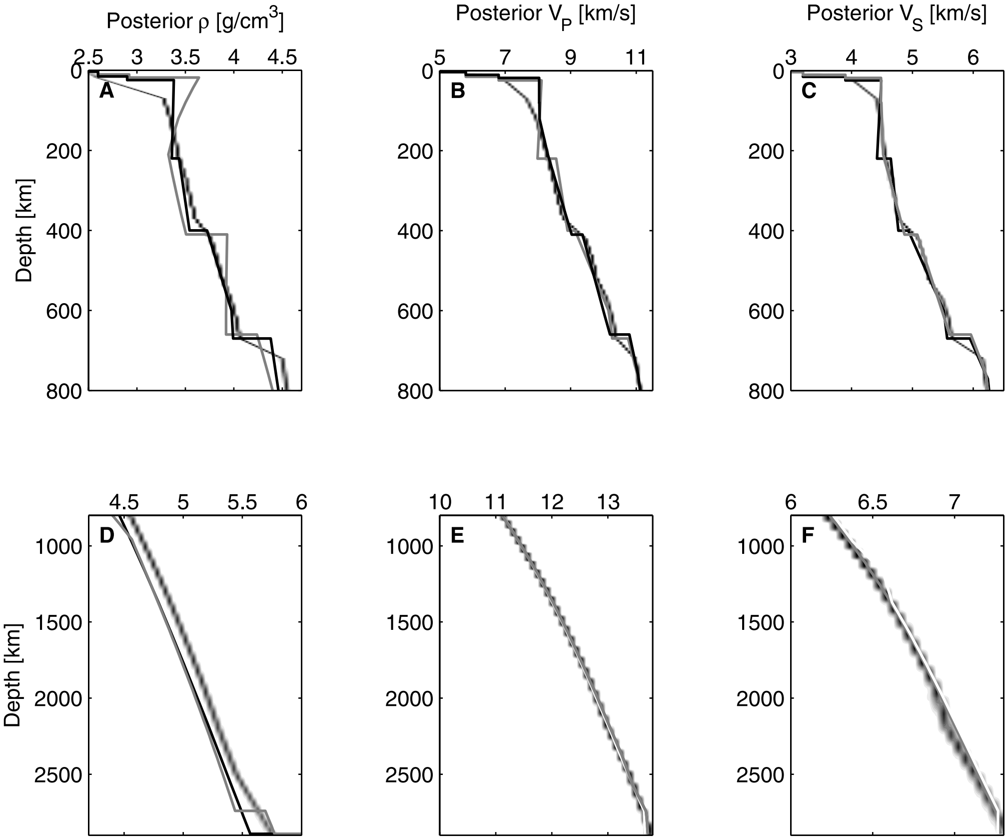

Figure 11. Sampled physical properties (posterior models only). (a–c) Radial profiles of ρ, V_P, and V_S in the upper mantle, transition zone, and uppermost lower mantle, and (d–f) lower mantle, respectively. For comparison, seismic reference models PREM (black line) and AK135 (gray line) are also shown. Shades of gray as before.

dertaking the same inversion as done here but using only elastic velocities to calculate traveltimes. Although we were able to fit data, within uncertainties, we found that the data fit had decreased overall. In addition, structure had been introduced into the traveltimes difference plots.

6.7. Physical Properties: Density, *P* and *S* Wave Velocity

[71] Other physical properties derived from the inversion include density and elasticity in the form of *P* and *S* wave velocities (Figure 11). These derived models are in good agreement with the purely seismologically derived models PREM and AK135.

6.8. Resolution, Stationarity and Parameter Trade-off

[72] A number of issues related to inverse problems in general need to be considered. These include questions of model parameterization (model parameter trade-off and uncertainty), data resolution and on a more technical note convergence and stationarity of the MCMC algorithm.

[73] As regards data resolution, we would like to know how sensitive inverted parameters are to individual data

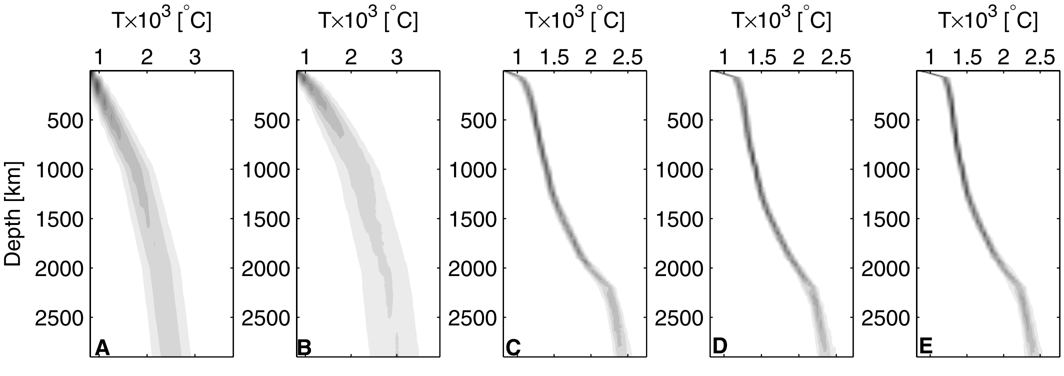

Figure 12. Posterior pdf's showing sampled geotherms obtained from inversion of (a) prior information, (b) geodetic data, (c) seismic data, and (d–e) inversion of both data sets using different random seeds. Shades of gray as before.

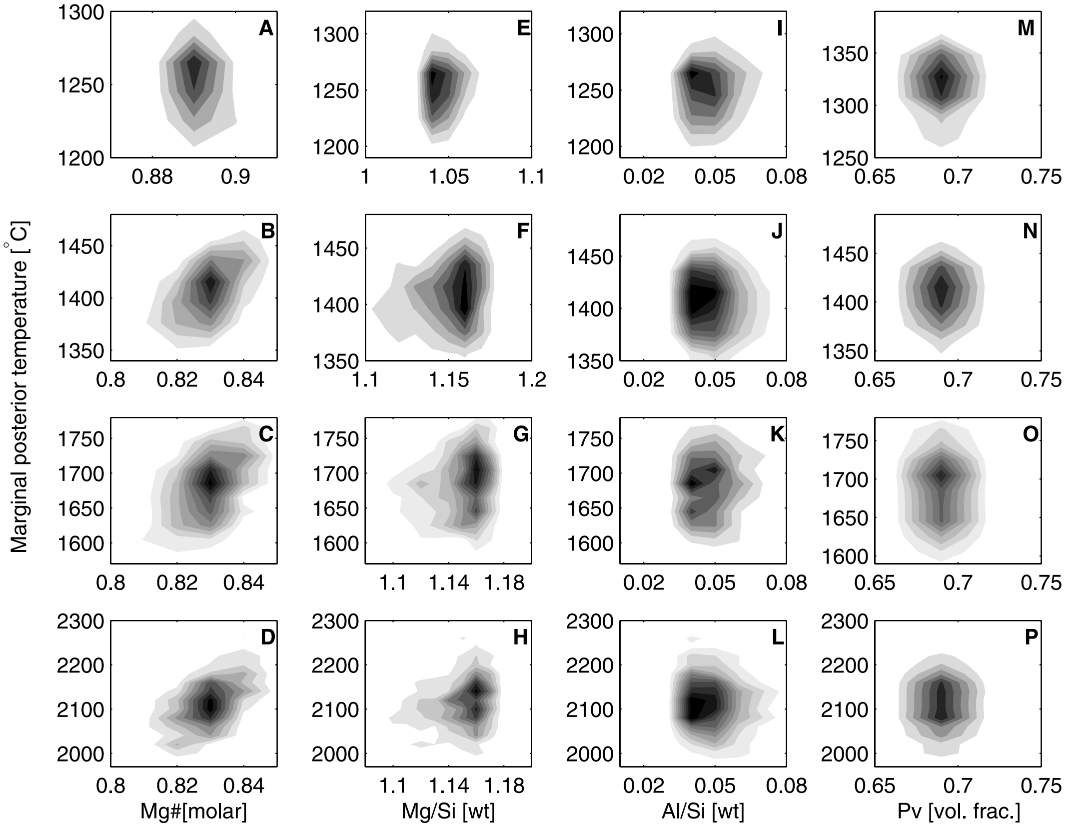

Figure 13. Posterior 2-D marginal pdf's showing trade-offs between inverted parameters as a function of depth. (a–d) Temperature versus Mg# ((Figure 13a) 500 km, (Figure 13b) 1000 km, (Figure 13c) 1600 km, (Figure 13d) 2100 km). (e–h) Temperature versus Mg/Si ratio (same depth intervals as for Figures 13a–13d). (i–l) Temperature versus Al/Si ratio (same depth intervals as for Figures 13a–13d). (m–p) Temperature versus Pv volume fraction ((Figure 13m) 800 km, (Figure 13n) 1000 km, (Figure 13o) 1600 km, (Figure 13p) 2100 km). Shades of gray as before.

sets. The answer is summarized in Figures 12a–12c, showing sampled geotherms (any other parameter could equally well have been chosen) for separate inversions of (1) prior information (same as Figure 7a), (2) geodetic data, and (3) seismic data. Significant narrowing of the prior pdf is seen in both cases (to increasing degree on going from geodetic to seismic data), implying that individual data sets can be used to constrain this parameter.

[74] There exist some qualitative criteria to assess whether the algorithm has converged and reached stationarity, which involve verifying that the estimated values of the model parameters sought have stabilized in a given run and checking that the same model parameter values are similar across independent chains. If this is satisfied, adequate confidence in the results is usually ensured. By comparing posterior geotherms (Figure 7b) with those obtained from two independent runs (inversion of all data using different random number sequences, Figures 12d–12e) shows that details vary, but that the overall characteristics are maintained, thus implying stationarity of the posterior pdf's.

[75] In interpreting results from inverse calculations one has to keep in mind that the model parameter values, their uncertainties and trade-offs are to a large extent determined by the chosen parameterization. There is no straightforward answer to the question of which parameterization to choose and that which is finally adopted usually reflects a subjective choice to an extent. Our choice of using three compositional and two core layers to model the Earth reflects an Occam's razor approach, as we asked ourselves what is the minimum number of layers needed to fit data, while maintaining a physically realistic model. Whichever parameterization is chosen, the probabilities calculated here are to be understood as mathematical entities that are based on (1) data and their uncertainties, (2) prior information as quantified here, and (3) the physical laws relating data and unknown model parameters employed.

[76] Another issue of importance is trade-off between inverted parameters. *Deschamps and Trampert* [2004], for example, found strong correlations between Fe content and temperature in the lower mantle, leading them to conclude that it is impossible to separate thermal from compositional effects. Here, we investigate several trade-offs among inverted parameters, specifically, T and c (Mg#, Mg/Si and Al/Si), T and mineralogy (Pv), as well as T and physical properties (not shown), at four different depths. The correlations are summarized in Figures 13a–13p. The investigated parameters are essentially uncorrelated, although Mg# and lower mantle temperatures seem to be slightly correlated. The overall uncorrelated nature of composition and temperature is expected, since c and T are distributed using independent prior pdf's. By further analyzing correlations of physical properties (e.g., V_S and ρ) versus c and T, we

observed the expected correlation between V_S and T, i.e., high T low V_S. Though small, the variations in physical properties V_S, for example, were found to be due to variations in composition (Fe, Mg and Si), as also observed earlier by *Trampert et al.* [2004]. The generally uncorrelated nature of c and T means that it is possible to separate thermal and compositional effects, contrary to some suggestions. We believe these differences to arise because of the different fundamental approaches which are taken, such as self-consistent thermodynamic phase equilibrium calculations versus parameterized phase diagram/EoS modeling, MCMC inversion versus random search.

7. Conclusion

[77] We have applied a self-consistent thermodynamical calculation which yields profiles of mineralogy and physical properties of the interiors of planets whose variations are described entirely by temperature, composition and pressure (depth). This enables us to confront, through a combination of the above with inverse methods, geophysical data directly with planetary compositional and thermal parameters. Moreover, the method allows us to naturally link different geophysical data in an inversion and it also provides a means of introducing additional information on various aspects of the media studied, such as geochemical, mineralogical and petrological, which are able to lead to further correlation of the geophysical data in the inversion. We have here demonstrated that fundamental information on the Earth can be produced to jointly yield plausible models of its composition, thermal, mineralogical and elastic properties, thus rendering it the most comprehensive analysis feasible to date. Given the general setup of the method, it is easily extended to encompass (1) other applications, i.e, data (normal modes, surface waves), (2) other methodologies (mantle anisotropy, seismic tomography, convection calculations), and (3) experimental data on more chemical components (e.g., Na_2O, H_2O) and complex systems (partial melt) as these become available.

[78] Specifically, the upper mantle compositions are found to be somewhat depleted in refractory elements (CaO and Al_2O_3) compared to the "standard" model of the Earth's primitive upper mantle composition by *McDonough and Sun* [1995]. Instead our geophysically derived models can be seen as reinforcing recent geochemically derived estimates by *Lyubetskaya and Korenaga* [2007]. The lower mantle appears to differ in composition from that of the upper mantle. We find a lower mantle composition that, relative to the upper mantle, is enriched in FeO, containing ~13 wt% as opposed to ~8 wt%. This is balanced by a lower SiO_2 content of ~42 wt% in comparison to ~47 wt% in the upper mantle. CaO and Al_2O_3 are also found to be somewhat higher in the lower mantle than in the upper, whereas MgO is within uncertainties of upper mantle estimates (ours as well as other literature estimates). This difference is also brought out in numbers such as Mg# and Mg/Si ratio, with the former being significantly lower (~0.84) and the latter higher (~1.2), respectively, than what is found for the primitive upper mantle (~0.89 and ~1.1). This means that the lower mantle does not act as a sink for Si as is often suggested in order to explain the discrepancy in Mg/Si ratio between upper mantle estimates and CI chondrites. As all the "missing" Si cannot be accommodated in the core, a relatively firm conclusion to be drawn here is that the Mg/Si ratio of the bulk silicate Earth composition relative to CI is higher and cannot be matched with any common class of chondrites. This is not too surprising as the asteroid belt is a very depleted quarry and its depletion dates long prior to the accretion of the Earth. The same arguments apply to the excess of Fe in our models, in that we wish to emphasize that the iron content of the Earth is a consequence of the accretion of the planet from a hierarchy of planetesimals that vary widely in metal content and Fe oxidation state. Thus it should not be surprising that the Earth's bulk Fe content and Fe/Mg ratio differs from that of CI.

[79] The lower mantle thermal state appears to deviate from an adiabat for depths >1300 km, with a geothermal gradient that is superadiabatic in the depth range ~1300–2500 km. The lower mantle is found to be neither "hot" nor "cool", with CMB temperatures around 2400°C. A thermal boundary layer seems to be present in the depth range 1800–2100 km, which might be related to the presence of chemical layers in the deeper mantle. However, boundaries or discontinuities associated with changes in physical properties in the lower mantle could not be located. The only transitions we found were located in the depth range 650–750, which is interpreted as implying that the 660 discontinuity is related to a change in chemistry. Given the reduced sensitivity of the data employed here to features such as deep mantle layering (other than D''), we leave it for future studies using other data to detect these.

[80] From the derived compositions and geotherms, and over equilibrium mineralogies, we have shown that our calculated physical properties (ρ, V_P, V_S, Q_S) agree with purely geophysically derived models such as PREM, AK135 and radial shear attenuation models obtained by various workers. The fact that our models agree with these geophysical models provides us with a strong measure of confidence that our approach employed here of jointly inverting different geophysical data directly for mantle composition and temperature, is not only feasible, but to be preferred to methods based solely on comparison of geophysical models with laboratory-based studies of physical properties.

[81] In closing we would like to note that we did attempt a joint inversion of the present data sets in combination with electromagnetic sounding data (the latter was inverted in a previous study of ours [*Khan et al.*, 2006b]). However, we found that it was not possible to fit all data sets jointly for any given combination of mantle composition and geotherm, because of incompatibility of the seismic and electromagnetic data sets. In addition to this, we also tried several different equations of state and parameterizations unsuccessfully. We believe that this is most probably related to the fact that laboratory-based electrical conductivity data for relevant, and especially lower, mantle minerals, are not as complete and well documented as is the case for elasticity data. It is nonetheless our hope that future studies will be able to resolve this difficulty, which probably hinges on amassing a much larger data set on the electrical conductivity of mantle minerals that considers in detail compositional effects, such as varying Fe and Al content, among others.

[82] **Acknowledgments.** We would like to thank I. Jackson and D. Anderson for their constructive reviews as well as Y. Fei for comments. Also, suggestions early on by S. Goes were helpful, as were those of H. Palme. Frederic Deschamps kindly provided his thermal model. Finally, A. Khan acknowledges support from the Danish Agency for Science, Technology and Innovation.

References

Allégre, C., J. P. Poirier, E. Humler, and A. W. Hofmann (1995), The chemical composition of the Earth, *Earth Planet. Sci. Lett.*, *134*, 515–526.

Anderson, D. L. (1989), *Theory of the Earth*, 366 pp., Blackwell, Oxford, UK.

Anderson, D. L. (2002), The case for irreversible chemical stratification of the mantle, *Int. Geol. Rev.*, *44*, 97–116.

Anderson, D. L. (2005), Self-gravity, self-consistency, and self-organization in geodynamics and geochemistry, in *Earth's Deep Mantle: Structure, Composition, and Evolution*, edited by R. D. van der Hilst, 165 pp., *Geophys. Monogr. Ser.*, vol. 160, pp. 165–186, AGU, Washington, D. C.

Anderson, D. L., and J. W. Given (1982), Absorption band *Q* model for the Earth, *J. Geophys. Res.*, *87*, 3893–3904.

Anderson, D. L., and R. S. Hart (1978), Attenuation models of the Earth, *Phys. Earth Planet. Inter.*, *16*, 289–306.

Birch, F. (1952), Elasticity and constitution of the Earth's interior, *J. Geophys. Res.*, *57*, 227–286.

Bosch, M. (1999), Lithologic tomography: From plural geophysical data to lithology estimation, *J. Geophys. Res.*, *104*, 749–766.

Brodholt, J., G. Helffrich, and J. Trampert (2007), Chemical versus thermal heterogeneity in the lower mantle: The most likely role of anelasticity, *Earth Planet Sci. Lett.*, *262*, 429–437.

Brown, J. M., and T. J. Shankland (1981), Thermodynamic parameters in the Earth as determined from seismic profiles, *Geophys. J. R. Astron. Soc.*, *66*, 579–596.

Burbine, T. H., and K. M. O'Brien (2004), Determining the possible building blocks of the Earth and Mars, *Meteorit. Planet. Sci.*, *39*, 667–681.

Cammarano, F., S. Goes, A. Deuss, and D. Giardini (2005), Is a pyrolitic adiabatic mantle compatible with seismic data?, *Earth Planet. Sci. Lett.*, *232*, 227–243, doi:10.1016/j.epsl.2005.01.031.

Chambat, F., and B. Valette (2001), Mean radius, mass, and inertia for reference Earth models, *Phys. Earth Planet. Inter.*, *124*, 237–253.

Chambers, J. E. (2001), Making more terrestrial planets, *Icarus*, *152*, 205–224.

Connolly, J. A. D. (2005), Computation of phase equilibria by linear programming: A tool for geodynamic modeling and an application to subduction zone decarbonation, *Earth Planet. Sci. Lett.*, *236*, 524–541, doi:10.1016/j.epsl.2005.04.033.

Connolly, J. A. D., and D. M. Kerrick (2002), Metamorphic controls on seismic velocity of subducted oceanic crust at 100–250 km depth, *Earth Planet. Sci. Lett.*, *204*, 61–74.

da Silva, C. R. S., R. M. Wentzcovitch, A. Patel, G. D. Price, and S. I. Karato (2000), The composition and geotherm of the lower mantle: Constraints from the elasticity of silicate perovskite, *Phys. Earth. Planet. Inter.*, *118*, 103–109.

Deschamps, F., and J. Trampert (2004), Towards a lower mantle reference temperature and composition, *Earth Planet. Sci. Lett.*, *222*, 161–175, doi:10.1016/j.epsl.2004.02.024.

Dobson, D. P., and J. P. Brodholt (2000), The electrical conductivity of the lower mantle phase magnesiowüstite at high temperatures and pressures, *J. Geophys. Res.*, *105*, 531–538.

Drake, M. J., and K. Righter (2002), Determining the composition of the Earth, *Nature*, *416*, 39–44.

Durek, J. J., and G. Ekström (1996), A radial model of anelasticity consistent with long-period surface wave attenuation, *Bull. Seismol. Soc. Am.*, *86*, 144–158.

Dziewonski, A. M., and D. L. Anderson (1981), Preliminary reference Earth model, *Phys. Earth Planet. Inter.*, *25*, 297–356.

Engdahl, E. R., R. D. van der Hilst, and R. P. Buland (1998), Global teleseismic earthquake relocation with improved travel times and procedures for depth determination, *Bull. Seismol. Soc. Am.*, *88*, 722–743.

Fabrichnaya, O. (1998), The assessment of thermodynamic parameters for solid phases in the Fe-Mg-O and Fe-Mg-Si-O systems, *Calphad-Computer Coupling Of Phase Diagrams and Thermochemistry*, *22*, 85–125.

Fabrichnaya, O., and O. L. Kuskov (1994), Composition of the Moon: 1. Assessment of thermodynamic properties and reliability of phase relation calculations in the FeO-MgO-Al_2O_3-SiO_2 system, *Phys. Earth Planet. Inter.*, *83*, 175–196.

Goes, S., R. Govers, and P. Vacher (2000), Shallow mantle temperatures under Europe from *P* and *S* wave tomography, *J. Geophys. Res.*, *105*, 11,153–11,169.

Hart, S. R., and A. Zindler (1986), In search of a bulk-Earth composition, *Chem. Geol.*, *57*, 247–267.

Hastings, W. K. (1970), Monte Carlo sampling methods using Markov chains and their applications, *Biometrika*, *57*, 97–109.

Helffrich, G. R., and B. J. Wood (2001), The Earth's mantle, *Nature*, *412*, 501–507.

Irifune, T. (1994), Absence of an aluminous phase in the upper part of the Earth's lower mantle, *Nature*, *370*, 131–133.

Irifune, T., and M. Isshiki (1998), Iron partitioning in a pyrolite mantle and the nature of the 410 km seismic discontinuity, *Nature*, *392*, 702–705.

Ita, J., and L. Stixrude (1992), Petrology, elasticity, and composition of the mantle transition zone, *J. Geophys. Res.*, *97*, 6849–6866.

Ito, E., and E. Takahashi (1989), Postspinel transformations in the system Mg_2SiO_4-Fe_2SiO_4 and some geophysical implications, *J. Geophys. Res.*, *94*, 10,637–10,646.

Jackson, I. (1998), Elasticity, composition and temperature of the Earth's lower mantle: A reappraisal, *Geophys. J. Int.*, *134*, 291–311.

Jackson, I., J. D. Fitz Gerald, U. H. Faul, and B. H. Tan (2002), Grain-size-sensitive seismic wave attenuation in polycrystalline olivine, *J. Geophys. Res.*, *107*(B12), 2360, doi:10.1029/2001JB001225.

Jagoutz, E., H. Palme, H. Baddenhausen, K. Blum, M. Cendales, G. Dreibus, B. Spettel, H. Waenke, and V. Lorentz (1979), The abundances of major, minor and trace elements in the Earth's mantle as derived from primitive ultramafic nodules, *Proc. Lunar Planet. Sci. Conf.*, *10*, 2031–2050.

Jarosewich, E. (1990), Chemical analyses of meteorites: A compilation of stony and iron meteorite analyses, *Meteoritics*, *25*, 323–337.

Javoy, M. (1995), The integral enstatite chondrite model of the Earth, *Geophys. Res. Lett.*, *22*, 2219–2222.

Jeanloz, R. (1990), The nature of the Earth's core, *Ann. Rev. Earth Planet. Sci.*, *18*, 357–386.

Kanamori, H., and D. L. Anderson (1977), Importance of physical dispersion in surface wave and free oscillation problems, *Rev. Geophys.*, *15*, 105–112.

Karato, S.-I. (1993), Importance of anelasticity in the interpretation of seismic tomography, *Geophys. Res. Lett.*, *20*, 1623–1626.

Karato, S.-I., and H. Spetzler (1990), Defect microdynamics in minerals and solid state mechanisms of seismic wave attenuation and velocity dispersion in the mantle, *Rev. Geophys.*, *28*, 399–421.

Kellogg, L. H., B. H. Hager, and R. D. van der Hilst (1999), Compositional stratification in the deep mantle, *Science*, *283*, 1881–1884.

Kennett, B. L. N., E. R. Engdahl, and R. Buland (1995), Constraints on seismic velocities in the Earth from travel times, *Geophys. J. Int.*, *122*, 108–124.

Khan, A., and J. A. D. Connolly (2008), Constraining the composition and thermal state of Mars from inversion of geophysical data, *J. Geophys. Res.*, *113*, E07003, doi:10.1029/2007JE002996.

Khan, A., J. A. D. Connolly, J. Maclennan, and K. Mosegaard (2006a), Joint inversion of seismic and gravity data for lunar composition and thermal state, *Geophys. J. Int.*, *168*, 243–258, doi:10.1111/j.1365-246X.200603200.x.

Khan, A., J. A. D. Connolly, and N. Olsen (2006b), Constraining the composition and thermal state of the mantle beneath Europe from inversion of long-period electromagnetic sounding data, *J. Geophys. Res.*, *111*, B10102, doi:10.1029/2006JB004270.

Khan, A., J. A. D. Connolly, N. Olsen, and K. Mosegaard (2006c), Constraining the composition and thermal state of the Moon from an inversion of electromagnetic lunar day-side transfer functions, *Earth Planet. Sci. Lett.*, *248*, doi:10.1016/j.epsl.2006.04.008.

Korenaga, J. (2008), Urey ratio and the structure and evolution of Earth's mantle, *Rev. Geophys.*, *46*, RG2007, doi:10.1029/2007RG000241.

Kuskov, O. L., V. A. Kronrod, and H. Annersten (2006), Inferring upper-mantle temperatures from seismic and geochemical constraints: Implications for Kaapvaal craton, *Earth Planet. Sci. Lett.*, *244*, 133–154, doi:10.1016/j.epsl.2006.02.016.

Lawrence, J. F., and M. E. Wysession (2006), QLM9: A new radial quality factor (Q_μ) model for the lower mantle, *Earth Planet. Sci. Lett.*, *241*, 962–971, doi:10.1016/j.epsl.2005.10.030.

Lodders, K. (2000), An oxygen isotope mixing model for the accretion and composition of rocky planets, *Space Sci. Rev.*, *92*, 341–354.

Lyubetskaya, T., and J. Korenaga (2007), Chemical composition of Earth's primitive mantle and its variance: 1. Method and results, *J. Geophys. Res.*, *112*, B03211, doi:10.1029/2005JB004223.

Marton, F. C., and R. E. Cohen (2002), Constraints on lower mantle composition from molecular dynamics simulations of $MgSi_3$ perovskite, *Phys. Earth Planet. Inter.*, *134*, 239–252.

Matas, J., and M. S. T. Bukowinski (2007), On the anelastic contribution to the temperature dependence of lower mantle seismic velocities, *Earth Planet. Sci. Lett.*, *259*(1–2), 51–65, doi:10.1016/j.epsl.2007.04.028.

Matas, J., J. Bass, Y. Ricard, E. Mattern, and M. S. T. Bukowinski (2007), On the bulk composition of the lower mantle: Predictions and limitations from generalized inversion of radial seismic profiles, *Geophys. J. Int.*, *170*, 764–780, doi:10.1111/j.1365-246X.2007.03454.x.

Mattern, E., J. Matas, Y. Ricard, and J. Bass (2005), Lower mantle composition and temperature from mineral physics and thermodynamic modelling, *Geophys. J. Int.*, *160*, 973–990, doi:10.1111/j.1365-246X.2004.02549.x.

McDonough, W. F., and R. L. Rudnick (1998), Mineralogy and composition of the upper mantle, in *Ultrahigh Pressure Mineralogy: Physics and Chemistry of the Earth's Deep Interior*, *Rev. Mineral. Geochem.*, edited by R. J. Hemley, vol. 37, pp. 139–164, Mineral. Soc. of Am., Washington, D. C.

McDonough, W. F., and S. S. Sun (1995), The composition of the Earth, *Chem. Geol.*, *120*(3–4), 223–253.

Metropolis, N., A. W. Rosenbluth, M. N. Rosenbluth, A. H. Teller, and E. Teller (1953), Equation of state calculations by fast computing machines, *J. Chem. Phys.*, *21*, 1087–1092.

Minster, B., and D. L. Anderson (1981), A model of dislocation controlled rheology for the mantle, *Phil. Trans. R. Soc. London Ser. A.*, *299*, 319–356.

Montagner, J. P., and B. L. N. Kennett (1996), How to reconcile body-wave and normal-mode reference Earth models, *Geophys. J. Int.*, *125*, 229–248.

Mooney, W. D., G. Laske, and G. Masters (1998), CRUST 5.1: A global crustal model at 5° × 5°, *J. Geophys. Res.*, *103*, 727–747.

Mosegaard, K. (1998), Resolution analysis of general inverse problems through inverse Monte Carlo sampling, *Inverse Problems*, *14*, 405–426.

Mosegaard, K., and M. Sambridge (2002), Monte Carlo analysis of inverse problems, *Inverse Problems*, *18*, 29–54.

Mosegaard, K., and A. Tarantola (1995), Monte Carlo sampling of solutions to inverse problems, *J. Geophys. Res.*, *100*, 12,431–12,447.

Ono, S., and A. R. Oganov (2005), In situ observations of phase transition between perovskite and $CaIrO_3$-type phase in $MgSiO_3$ and pyrolitic mantle composition, *Earth Planet. Sci. Lett.*, *236*, 914–932, doi:10.1016/j.epsl.2005.06.001.

Palme, H., and K. G. Nickel (1985), Ca/Al ratio and composition of the Earth's primitive upper mantle, *Geochim. Cosmochim. Acta*, *49*, 2123–2132.

Palme, H., and H. St. C. O'Neill (2003), Cosmochemical estimates of mantle composition, in *Treatise on Geochemistry*, edited by H. D. Holland and K. H. Turekian, pp. 1–38, Elsevier, New York.

Palme, H., H. St. C. O'Neill, and W. Benz (2003), Evidence for collisional erosion of the Earth, *Lunar Planet. Sci. Conf.*, *34*, Abstract 1741.

Poirier, J. P. (1994), Light elements in the Earth's outer core: A critical review, *Phys. Earth Planet. Inter.*, *85*, 319–337.

Ricard, Y., E. Mattern, and J. Matas (2005), Synthetic tomographic images of slabs from mineral physics, in *Earth's Deep Mantle: Structure, Composition, and Evolution*, *Geophys. Monogr. Ser.*, vol. 160, edited by R. D. van der Hilst, pp. 283–300, AGU, Washington, D. C.

Ringwood, A. E. (1975), *Composition and Petrology of the Earth's Mantle*, 618 pp., McGraw-Hill, New York.

Romanowicz, B., and J. J. Durek (1999), Attenuation in the Earth: A review, in *Earth's Deep Interior: Mineral Physics and Tomography From the Atomic to the Global Scale*, *Geophys. Monogr. Ser.*, edited by S.-I. Karato et al., pp. 161–180, AGU, Washington, D. C.

Salters, V. J. M., and A. Stracke (2004), Composition of the depleted mantle, *Geochem. Geophys. Geosyst.*, *5*, Q05B07, doi:10.1029/2003GC000597.

Sobolev, S. V., and A. Y. Babeyko (1994), Modeling of mineralogical composition, density and elastic-wave velocities in anhydrous magmatic rocks, *Surv. Geophys.*, *15*, 515–544.

Stacey, F. D., and P. M. Davis (2004), High pressure equations of state with applications to the lower mantle and core, *Phys. Earth Planet. Inter.*, *142*, 137–184, doi:10.1016/j.pepi.2004.02.003.

Stixrude, L., and C. Lithgow-Bertelloni (2005a), Mineralogy and elasticity of the oceanic upper mantle: Origin of the low-velocity zone, *J. Geophys. Res.*, *110*, B03204, doi:10.1029/2004JB002965.

Stixrude, L., and C. Lithgow-Bertelloni (2005b), Thermodynamics of mantle minerals: I. Physical properties, *Geophys. J. Int.*, *162*, 610–632.

Stixrude, L., and C. Lithgow-Bertelloni (2007), Influence of phase transformations on lateral heterogeneity and dynamics in Earth's mantle, *Earth Planet. Sci. Lett.*, *263*, 45–55, doi:10.1016/j.epsl.2007.08.027.

Tarantola, A. (2004), *Inverse Problem Theory and Model Parameter Estimation*, Soc. for Ind. and Appl. Math., Philadelphia.

Tarantola, A., and B. Valette (1982a), Generalized nonlinear inverse problems solved using the least squares criterion, *Rev. Geophys.*, *20*, 219–232.

Tarantola, A., and B. Valette (1982b), Inverse problems: Quest for information, *J. Geophys.*, *50*, 159–170.

Taylor, S. R. (1979), Lunar and terrestrial potassium and uranium abundances: Implications for the fission hypothesis, *Proc. Lunar Planet. Sci. Conf.*, *10*, 2017–2030.

Taylor, S. R. (1980), Refractory and moderately volatile element abundances in the Earth, Moon and meteorites, *Proc. Lunar Planet. Sci. Conf.*, *11*, 333–348.

Trampert, J., F. Deschamps, J. Resovsky, and D. Yuen (2004), Probabilistic tomography maps chemical heterogeneities throughout the lower mantle, *Science*, *306*, 853–856.

van der Hilst, R. D., S. Widiyantoro, and E. R. Engdahl (1997), Evidence for deep mantle circulation from global tomography, *Nature*, *386*, 578–584.

Weidenschilling, S. J. (2000), Formation of planetesimals and accretion of the terrestrial planets, *Space Sci. Rev.*, *92*, 295–310.

Wetherill, G. W. (1994), Provenance of the terrestrial planets, *Geochim. Cosmochim. Acta*, *58*, 4513–4520.

Widmer, R., G. Masters, and F. Gilbert (1991), Spherically symmetric attenuation within the Earth from normal mode data, *Geophys. J. Int.*, *104*, 541–553.

Wood, B. J., M. J. Walter, and J. Wade (2006), Accretion of the Earth and segregation of its core, *Nature*, *441*, 825–833.

Xu, Y., T. J. Shankland, and B. T. Poe (2003), Correction to "Laboratory-based electrical conductivity in the Earth's mantle", *J. Geophys. Res.*, *108*(B6), 2314, doi:10.1029/2003JB002552.

Zerr, A., and R. Boehler (1993), Melting of (Mg, Fe)SiO_3-perovskite to 625 kilobars: Indication of a high melting temperature in the lower mantle, *Science*, *262*, 553–555.

Zerr, A., and R. Boehler (1994), Constraints on the melting temperature of the lower mantle from high-pressure experiments on MgO and magnesiowüstite, *Nature*, *371*, 506–508.

J. A. D. Connolly, Earth Sciences Department, Swiss Federal Institute of Technology, Songstresses 5, CR-8092 Zurich, Switzerland. (james.connolly@erdw.ethz.ch)

A. Khan, Niels Bohr Institute, University of Copenhagen, Julian Maries Vej 30, DK-2100 Copenhagen, Denmark. (amir@gfy.ku.dk; klaus@gfy.ku.dk)

S. R. Taylor, Department of Earth and Marine Sciences, Australian National University, Canberra ACT 2601, Australia. (ross.taylor@anu.edu.au)